Calculation tool for estimation of the material properties of glulam beams with known layout

Mariia Martus

School of Engineering

Thesis submitted for examination for the degree of Master of Science in Technology.
Espoo 31.7.2020

Supervisor

Prof. Gerhard Fink

Advisor

M.Sc. Joonas Jaaranen

Aalto University
School of Engineering

Aalto University
School of Engineering

Aalto University, P.O. BOX 11000, 00076 AALTO
www.aalto.fi
Abstract of the master's thesis

Author Mariia Martus

Title Calculation tool for estimation of the material properties of glulam beams with known layout

Master programme Building technology **Code** ENG27

Supervisor Prof. Gerhard Fink

Advisor M.Sc. Joonas Jaaranen

Date 31.7.2020 **Number of pages** 47+15 **Language** English

Abstract

Properties of glued laminated timber are subjected to large uncertainties. To increase material reliability and utilization ratio, these uncertainties should be handled more efficiently. The aim of this study was to develop a tool for reliable prediction of load-bearing capacity of glulam beams with well-known properties. Different models were applied in Monte-Carlo simulation framework and their performance were evaluated on the set of tested beams from literature. Prediction of bending strength as well as estimation of failure initiation location were of special interest. Using transformed cross-section method, influence of strength, stiffness and finger joint material models to the glulam properties estimation was evaluated. It was found that for better strength prediction lamination effect should be additionally taken into account in exploited lamination strength model. Simulation with this calibration gave significantly improved strength prediction for the beams. Established simple isotropic FEM model showed similar results as transformed cross-section method. When orthotropic material model was utilized, lower strength of beams was predicted. By means of fictitious crack approach in Abaqus, crack propagation and branching in glulam beams in bending were simulated. Established FEM model allowed simulation of progressive failure, however still leaving room for improvement in the strength prediction regard.

Keywords timber, glulam, transformed cross-section method, FEM, Hashin's failure, Abaqus

Contents

1 Introduction

Glued laminated timber is wood product made of boards glued together. Properties of glulam beams depend on the properties of composing boards and their arrangement in the beam. Prediction of such glulam properties as strength and stiffness is non-trivial task due to high between- and within board natural variability of wood properties. One of the ways to evaluate strength and stiffness of glulam beam is establish a model which defines beam properties from properties of individual boards and its setup. More precise prediction of GLT performance will contribute to more efficient and safer use of the material.

Aim of the work

The aim of this work is to develop a tool for reliable prediction of glulam beams properties in bending based on properties of its laminations and setup. For design purposes it is necessary to know characteristic strength values of structural members. That is why prediction of probabilistic distribution of properties is of interest. The question is – how well is it possible to predict beam properties based on scanned data. The influence of material properties on the post-fracture behavior and load-bearing capacity as well as cracking pattern prediction are also in the focus of the thesis.

Methods

To be used in construction, structural timber is graded first. Modern machine grading devices able not only to estimate the board class, but also to give information about local board properties with high resolution. Material models, described in Fink (2014), is used to estimate lamination mechanical properties. Based on this data, two methods are used to predict beam properties:

- transformed cross-section (TS) method based on beam theory – the simple and computationally inexpensive, done with Matlab
- finite element method (FEM) employing different failure mechanisms, Abaqus software was used

Glulam properties are simulated with Monte-Carlo method. Obtained strength and stiffness probabilistic distributions, as well as predicted fracture development, are evaluated against tests on full-scale glulam beams described in Fink et al. (2013) and Stadelmann (2015). By means of fast TS method performance of variations of material models is estimated. FEM simulation aiming to capture post-fracture behavior of GLT is established. Due to high computational volume, Python scripting is widely used.

Content of the thesis

In Chapter 2 background information relevant for the topic is given, which includes three main parts: timber and GLT as a material, overview of existing glulam models,

fracture behavior of timber and its modeling. In Chapter 3 experimental data on which models are used is presented. Chapter 4 contains discussion about material models for timber properties used in simulations. Glulam models evaluated in chapter 5 include In Chapter 5 variations of TS and FEM models is applied and its results are presented. Influence of mesh size in FEM modeling is evaluated. Chapter 6 contains conclusions from the work done. In Appendices results of simulations with glulam models are presented graphically.

2 Background

In this chapter overview is given for relevant topics concerning this thesis. Definition of glulam is given, timber and GLT as a material is outlined. Existing glulam models are briefly described, fracture behavior of timber and its modeling in Abaqus is addressed.

2.1 Glued laminated timber as a material

Glued laminated timber, GLT or glulam - is an engineered wood product developed in the end of 19th century. To produce glulam beams boards of thickness 30-50 mm are used. They are finger jointed together to produce continuous lamella and cut into beam length pieces. These boards then planed from the top and bottom sides and glued together under pressure into straight or curved shape element. The beam is then planed from sides to have better visual appearance. The size of the beams is restricted by the available press size and transportation facilities.

GLT can form members of size and shape impossible for solid wood. It also facilitates usage of lower-grade lumber in less stressed regions of structural members. GLT exhibits higher mechanical properties in comparison with boards due to lamination effects.

GLT is made from wood - naturally grown material. Speaking about wood properties, distinction should be made for clear wood and structural timber properties. Clear defect-free wood can be treated as anisotropic material in longitudinal (L), radial (R) and tangential (T) direction. Wood properties in radial and tangential directions are quite similar and significantly less than in longitudinal direction. For example, tension strength in longitudinal direction can be 30-50 times higher and elastic modulus 50-80 times higher than in transversal directions (Thelandersson & Larsen 2003). In many applications wood is simulated as transversely orthotropic material, with same properties in radial and tangential direction. For the plane stress case, the constitutive relationship is

$$\begin{Bmatrix} \epsilon_1 \\ \epsilon_2 \\ \epsilon_3 \end{Bmatrix} = \begin{pmatrix} 1/E_1 & -\nu_{12}/E_1 & 0 \\ -\nu_{12}/E_1 & 1/E_2 & 0 \\ 0 & 0 & 1/G_{12} \end{pmatrix} \begin{Bmatrix} \sigma_{11} \\ \sigma_{22} \\ \tau_{12} \end{Bmatrix} \tag{1}$$

where ϵ, σ, τ are strain and stress components, E_1, E_2 are modulus of elasticity (MOE) along and perpendicular to the grain, G_{12} is shear modulus and ν_{12} is Poisson ratio.

Mechanical behavior of the GLT beam as a whole is determined by properties of its components: timber boards, finger joints and glue-lines between the boards. The thesis focuses on the influence of the timber boards properties and arrangement to the load-bearing capacity of the beams. According to Euler-Bernoulli bending theory, the bending stresses over the whole cross-section can be subdivided into normal and bending stresses in laminations. Bending stress in a single lamella is relatively small in comparison with normal stress, especially for outer laminations. Bending stress σ_m can be approximated with axial stress in laminations σ_t in GLT

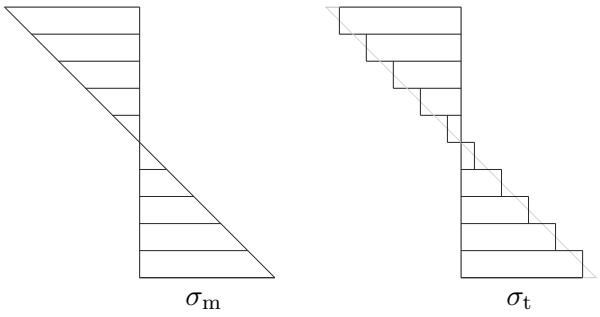

Figure 1: Bending stresses within a cross-section and its approximation with normal stresses. From Fink (2014)

beams with numerous lamellas (Fig. 1). That is why tensile strength of the boards is important for beam strength prediction.

Timber boards consist not only of clear wood. They are produced by cutting of the tree trunk and contain defects including knots, spiral grain and compression wood. Thus, timber as a material is inhomogeneous and has significant variability of properties. Variability is observed between different species, different growth areas, in between boards from the same location as well as variability of the properties along the board length. To ensure required load bearing capacity of the material, the timber is graded based on strength and stiffness indicators. Knots, spiral grain, density, annual rings thickness, modulus of elasticity and their combinations can be used to estimate board properties. Standing alone, MOE correlates with strength the most as it is influenced by the clear wood properties as well as timber defects. Static MOE is defined by loading a board and measuring its displacement or vice versa. Dynamic MOE is usually determined with transient excitation frequency method. In the thesis dynamic MOE and X-ray measurements for knottiness were used as strength and stiffness indicators (E_m and K_m).

Lamination effect

As was explained in the previous section, bending stresses in a beam can be approximated with tensile stresses of its lamellas. However, bending strength of the glulam in most cases is higher than tensile strength of boards it is made from. This is called laminating effect and quantitatively described with laminating factor k_{lam}:

$$k_{lam} = \frac{f_{m,g}}{f_{t,lam}} \tag{2}$$

where $f_{m,g}$ is bending strength of the glulam beam by ordinary beam theory and $f_{t,lam}$ is tensile strength of the source lumber. Explanation of the lamination effect is given in Falk & Colling (1995) by:

– Effect of tension test procedure: In tension test for boards, lateral movements due to unsymmetrical stiffness of the board is not restrained, thus appearing

bending moment decreases tensile strength. In glulam adjacent laminations restrict sideway deformation and bending load is not induced.

– Reinforcement of defects: Weaker cross-sections usually are less stiff and reinforced with adjacent stiffer lamellas. Stress redistributes to stiffer and usually stronger element. It worth to mention as a side note, that according to Serrano & Larsen (1999) stress redistribution around short weak sections is not as pronounce as predicted by beam theory.

– Dispersion effect: in glulam, the probability of a defect having a serious influence on the strength of the beam is smaller than in single lamination.

Lamination effect is larger for laminations of lower grade. In low quality lumber with bigger knots, distortion during the test is more significant and reinforcing effect is stronger. Coefficient of variation of the lamination strength is higher than of the glulam strength. That makes lamination effect more pronounced on the characteristic strength than on the mean strength.

Size and load configuration effects

Strength of timber, as it behaves brittle in tension, depends on the size of the element. It is commonly explained with Weibull weakest link theory. The theory states that a structural element fails when its weakest part fails. With increasing size of element the probability of occurrence of severely weak section also increases thus decreasing element's strength. The size effect is often expressed through size factor k_{vol}, Eq. (3). It shows the relation between strength of the same material in elements of different volumes.

$$k_{vol} = \left(\frac{V}{V_0}\right)^n, \; n < 0 \tag{3}$$

where V is the volume of the specimen and V_0 is the reference volume. According to Thelandersson & Larsen (2003) $-0.4 < n < -0.1$.

The load configuration effect is based on the similar principle; the volume of the maximally stressed material depends on the loading. Probability, that stress overcome stochastic value of material strength at some point, increases with considered volume. For example, strength of GLT in pure tension statistically will be lower than in bending. In tension the whole volume is checked for maximum stress, whereas in bending it is only the lowest lamella. For the same reason, beams under constand bending moment show lower bending strength than in four point bending test.

2.2 Glulam models

Load-bearing capacity of GLT and its characteristic values have been widely studied. Two main ways to evaluate characteristic bending strength $f_{m,g,k}$ and define strength distribution accurately are experimental investigations and simulation models. List of experimental models for prediction of glulam bending strength based on tensile strength of boards can be found for example in Brandner & Schickhofer (2008). To

make reliable statistical models for every beam size and grade configuration many experiments are needed; simulation models are less costly approach. Two selected models, relevant for the study, are described in this chapter, based on Thelandersson & Larsen (2003) and Hernandez et al. (1992).

Most models consist of two main parts - defining stochastic properties of the material and evaluating mechanical performance of the glulam beam. The focus of this thesis is more on the latter.

Transformed section method

Transformed section method is the base of the model also known as PROLAM. In order to apply simple beam formulas to inhomogeneous glulam beam the method transform the width of each piece of lamella according to its stiffness. Assuming that plane sections perpendicular to beam axis remains plane one can calculate stress at any height in cross-sections along the beam axis:

$$\sigma(y) = \frac{M}{EI} \cdot y \cdot E(y) \tag{4}$$

where y is the distance between neutral axis and point under consideration, M is bending moment in the cross-section, EI is cross-section rigidity and $E(y)$ is stiffness of the layer under consideration.

When normal stress under the load in some element exceeds strength of the material, the element considered failed, it is assigned zero MOE and calculation is repeated. First failed element not necessary corresponds to maximum load bearing capacity of the beam. In PROLAM tool failure process propagates while next element fails under bigger load then any of previous ones (Hernandez et al. 1992).

To estimate the bending stiffness of the beam, for example with Eq. (22), deflection at the mid span is calculated using complementary virtual work principle with Eq. 5.

$$\Delta = \sum_{i=1}^{n} \left(\frac{M_i m_i}{EI_i} \cdot dx + \frac{k V_i v_i}{GA_i} \cdot dx \right) \tag{5}$$

where M_i is bending moment in i$^{\text{th}}$ cross-section from applied load, m_i is bending moment from vertical unit force applied in the middle of the beam, EI_i is bending rigidity of transformed cross-section, V_i is shear force from applied load, v_i is shear force from vertical unit force applied in the middle of the beam, GA_i is shear rigidity of transformed cross-section, dx is length increment at which calculations are performed and k is form factor. $k = 1.2$ for rectangular section. First part of the sum gives bending deflection, second - takes shear deflection into account.

Model's advantage is that it is computationally light while being quite accurate. However, it does not take into account stress concentrations around weak elements, which take place according to Serrano & Larsen (1999), does not reflect interactions between neighboring cross sections, just simple linear elastic material model is used and assumption about plane cross-sections does not precisely hold in reality, as could be seen for example from Fink et al. (2013).

FEM-based calculation models

Foschi & Barrett (1980) used finite element method and Monte-Carlo simulation to calculate strength and stiffness and its probability distributions for glulam beams. Laminations were subdivided to 150 mm long finite elements and with linear elastic analysis load-bearing capacity with brittle failure was calculated. Ehlbeck et al. (1985) improve the model by incorporating finger joint properties to the model and simulating progressive failures. Regression model was used to generate FJ properties based on densities of adjacent laminations. Progressive failure was modeled by removing failed elements from calculation. This model is known as "Karlsruhe calculation model".

2.3 Fracture in timber

Mechanical behavior of cracks and notches usually cannot be well predicted with usual maximum stress design approach. These sharp changes in geometry introduce stress singularities in the structure. It means that according to plain mechanics equations, stress at the crack tip should approach infinity, which is not practically true. Fracture mechanics approaches were developed to deal with singularities. Overview of fracture mechanics strength analysis methods used in recent years is presented by Serrano & Gustafsson (2006). Failure criteria used in fracture mechanics is expressed in terms of the energy release during the propagation of pre-existing crack or with stress intensity factor. Corresponding critical energy release rate G_c and critical stress intensity factor K_c is considered to be a material property. Formulas for conversion of stress concentrate coefficient K_{Ic} to fracture energy G_{Ic} can be found for example in Jernkvist (2000).

Crack propagation in timber is marked with two letters: first denotes the direction normal to the crack plane and second is the direction of crack growth (Fig. 2). There

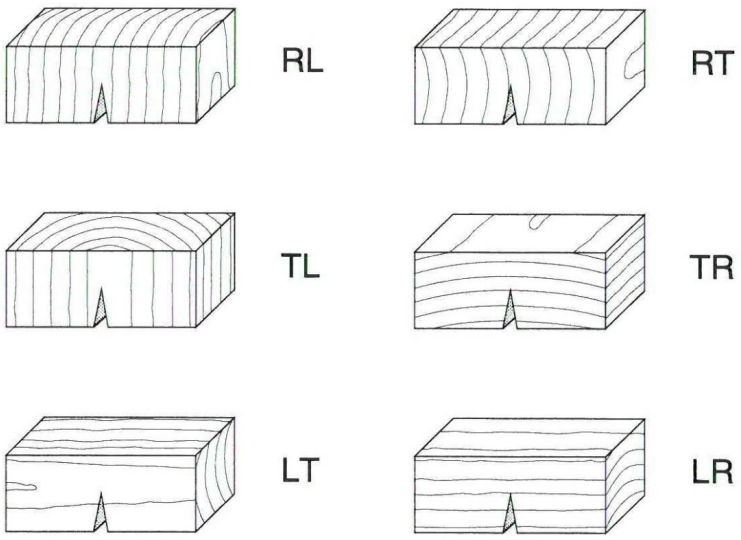

Figure 2: The six principal systems of cracking in wood. From Jernkvist (2000)

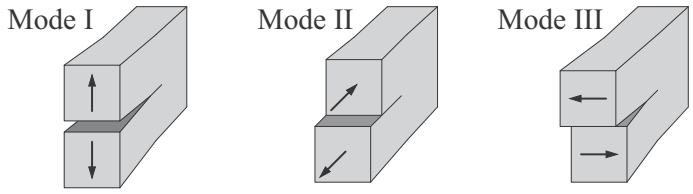

Figure 3: The three fracture modes: opening mode (mode I), sliding mode (mode II), and tearing mode (mode III). From Danielsson (2013)

are three modes of crack growth (Fig. 3): opening (Mode I), sliding (Mode II) and tearing (Mode III). Fracture mechanisms in these modes are not the same, so critical fracture energies and stress-displacement curves is usually also different and marked as G_{Ic}, G_{IIc} and G_{IIIc}. Often in the structure some combination of these modes takes place.

2.4 Failure criteria

Failure in timber is complex combination of fracture along and across the grain in tension and shear. Common approach to predict failure in complex stress states is to use failure criteria with values of strength in simpler stress states. A few widely used criteria are shown here.

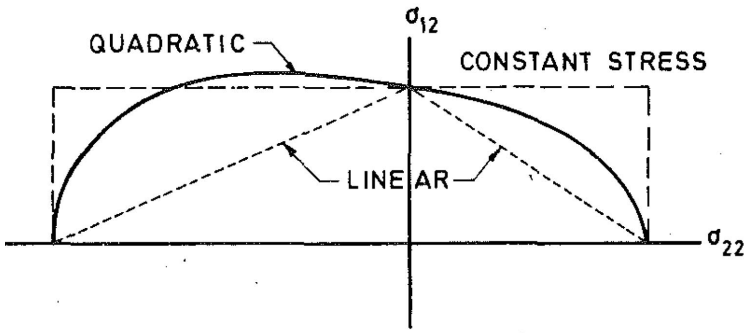

Figure 4: Failure surfaces - schematic. From Hashin (1980)

Maximum principal stress criteria

Constant stress, or maximum principal stress criteria, Eq. (6), assumes that material fail when any of its principal stresses reach the limit, see Fig. 4. Material strength is overestimated commonly with this criteria under combined stress states.

$$max\left(\frac{\sigma_{11}}{X}, \frac{\sigma_{22}}{Y}, \left|\frac{\tau_{12}}{S}\right|\right) = 1 \tag{6}$$

Linear failure criteria

To take into account interaction of spatial stresses, linear failure criteria could be used, Eq. (7). For most of materials this criteria is very conservative.

$$\frac{\sigma_{11}}{X} + \frac{\sigma_{22}}{Y} + \frac{\tau_{12}}{S} = 1 \tag{7}$$

Quadratic criteria

Most failure criteria are quadratic polynomials. The simplies of them is shown in Eq. (8). It forms an elliptic failure surface.

$$\left(\frac{\sigma_{11}}{X}\right)^2 + \left(\frac{\sigma_{22}}{Y}\right)^2 + \left(\frac{\tau_{12}}{S}\right)^2 = 1 \tag{8}$$

Hashin's criteria

Wood can be considered as unidirectional composite, and have different failure mechanisms and stresses along and across the grain. Hashin (1980) develop separate failure criteria for fiber and matrix modes in tension and compression stress states. Thus failure surface is piecewise smooth. With plane stress assumption Hashin's criteria:

In fiber tension mode ($\sigma_{11} \geq 0$):

$$\left(\frac{\sigma_{11}}{X^T}\right)^2 + \left(\frac{\tau_{12}}{S^L}\right)^2 = 1 \qquad \text{or} \qquad \sigma_{11} = X^T \tag{9}$$

In fiber compression mode ($\sigma_{11} \leq 0$):

$$\sigma_{11} = X^C \tag{10}$$

In matrix tension mode ($\sigma_{22} \geq 0$):

$$\left(\frac{\sigma_{22}}{Y^T}\right)^2 + \left(\frac{\tau_{12}}{S^L}\right)^2 = 1 \tag{11}$$

In matrix compression mode ($\sigma_{22} \leq 0$):

$$\left(\frac{\sigma_{22}}{2S^T}\right)^2 + \left[\left(\frac{Y^C}{2S^T}\right)^2 - 1\right]\frac{\sigma_{22}}{Y^C} + \left(\frac{\tau_{12}}{S^L}\right)^2 = 1 \tag{12}$$

where X^T is longitudinal tensile strength, X^C is longitudinal compressive strength, Y^T is transverse tensile strength, Y^C is transverse compressive strength, S^L is longitudinal shear strength and S^T is transverse shear strength.

2.5 Damage modeling with Hashin's criteria in Abaqus

In Abaqus damage for fiber-reinforced composites can be modeled as Hashin damage. For detailed description, see Abaqus Manual (2013). Hashin's failure criteria Eq. (9)-(12) is used as damage initiation criteria.

Fiber tension($\hat{\sigma}_{11} \geq 0$):

$$F_f^t = \left(\frac{\hat{\sigma}_{11}}{X^T}\right)^2 + \alpha \left(\frac{\hat{\tau}_{12}}{S^L}\right)^2 \tag{13}$$

Fiber compression ($\hat{\sigma}_{11} \leq 0$):

$$F_f^c = \left(\frac{\hat{\sigma}_{11}}{X^C}\right)^2 \tag{14}$$

Matrix tension ($\hat{\sigma}_{22} \geq 0$):

$$F_m^t = \left(\frac{\hat{\sigma}_{22}}{Y^T}\right)^2 + \left(\frac{\hat{\tau}_{12}}{S^L}\right)^2 \tag{15}$$

Matrix compression ($\hat{\sigma}_{22} \leq 0$):

$$F_m^c = \left(\frac{\hat{\sigma}_{22}}{2S^T}\right)^2 + \left[\left(\frac{Y^C}{2S^T}\right)^2 - 1\right]\frac{\hat{\sigma}_{22}}{Y^C} + \left(\frac{\hat{\tau}_{12}}{S^L}\right)^2 \tag{16}$$

Where α is a coefficient that determines the contribution of the shear stress to the fiber tensile initiation criterion, $\hat{\sigma}_{11}, \hat{\sigma}_{22}, \hat{\tau}_{12}$ are components of the effective stress tensor, that is used to evaluate the initiation criteria.

Effective stress tensor components are computed from

$$\hat{\sigma} = \boldsymbol{M}\sigma \tag{17}$$

with σ denoting true stress, $\boldsymbol{M}$ - damage operator

$$\boldsymbol{M} = \begin{bmatrix} \frac{1}{1-d_f} & 0 & \\ 0 & \frac{1}{1-d_m} & 0 \\ 0 & 0 & \frac{1}{1-d_s} \end{bmatrix} \tag{18}$$

where d_f, d_m and d_s are internal fiber, matrix and shear damage variables. They are derived from damage variables $d_f^t, d_f^c, d_m^f, d_m^c$ - fiber tensile and compressive, matrix tensile and compressive damage, from corresponding failure modes as follow:

$$\begin{gathered} d_f = \begin{cases} d_f^t & \text{if } \hat{\sigma}_{11} \geq 0, \\ d_f^c & \text{if } \hat{\sigma}_{11} \leq 0 \end{cases} \\ d_m = \begin{cases} d_m^t & \text{if } \hat{\sigma}_{22} \geq 0, \\ d_m^c & \text{if } \hat{\sigma}_{22} \leq 0 \end{cases} \\ d_s = 1 - (1 - d_f^t)(1 - d_f^c)(1 - d_m^t)(1 - d_m^c) \end{gathered} \tag{19}$$

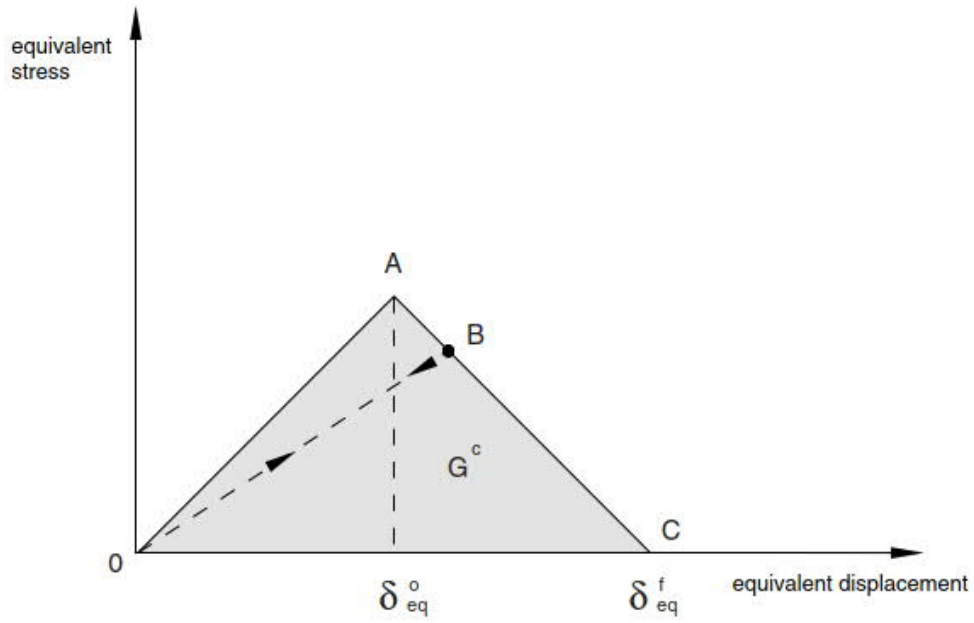

Figure 5: Linear damage evolution. From Abaqus Manual (2013)

Once the element reachs any of failure criteria, its corresponding damage variable may only increase. It changes in such a manner that equivalent stress depends on equivalent displacement according to Fig. 5. Displacement δ_{eq}^{o} is a function of strength, stiffness of the material and finite element size, δ_{eq}^{f} is defined so that fracture energy is the area OAC under the stress-displacement curve. Equivalent stress and displacement are introduced to alleviate the influence of mesh size. For more detail on it and on computing damage variables see (Abaqus Manual 2013, 24.3.3).

At every iteration response of the material is computed from

$$\sigma = \boldsymbol{C_d}\epsilon \tag{20}$$

Elasticity matrix here takes damage into account and defined as

$$\boldsymbol{C_d} = \frac{1}{D}\begin{bmatrix} (1-d_f)E_1 & (1-d_f)(1-d_m)\nu_{12}E_1 & 0 \\ (1-d_f)(1-d_m)\nu_{12}E_2 & (1-d_m)E_2 & 0 \\ 0 & 0 & (1-d_s)GD \end{bmatrix} \tag{21}$$

with $D = 1-(1-d_f)(1-d_m)\nu_{12}\nu_{21}$.

3 Initial data

In this section glulam beams tests from few sources are presented. In the rest of the thesis these beams was modeled with different techniques.

3.1 Experimental data

36 beams of Norway spruce in total were tested in Zurich ETH by G. Fink (24 beams) and P. Stadelmann (12 beams). Test reports and details see in Fink et al. (2013) and Stadelmann (2015).

Beams were produced from boards scanned and graded with a Goldeneye-706 device into two strength grades: L25 and L40 according to SFS-EN 14081-4 (2009). Schematic illustration of the test setups are shown in Fig. 6. Structural dimensions and certain test results are presented in Table 1.

Bending stiffness of the beams, presented in the table, was calculated according to SFS-EN 408 (2012), Eq. (22), and bending strength according to SFS-EN 408 (2012), Eq. (23).

$$E_{m,g} = \frac{3al^2 - 4a^3}{2bh^3\left(2\frac{\omega_2-\omega_1}{F_2-F_1} - \frac{6a}{5Gbh}\right)} \tag{22}$$

$$f_m = \frac{3Fa}{bh^2} \tag{23}$$

where $E_{m,g}$ is global bending stiffness, a is distance between the load application point and the nearest support, l is span length, b is width of the cross section, h is height of the cross section, $(F_2 - F_1)$ id load increase within the load interval between $[0.1,\ 0.4]F_u$, $(\omega_2 - \omega_1)$ is deformation increase within the load interval between $[0.1,\ 0.4]F_u$, G is shear modulus. Shear modulus was taken as 650 MPa.

3.2 Observed failure mechanisms

Bending failure of glulam beams is associated with brittle rupture of tensioned lamellas because in compression timber has ductile behavior. Although it is not possible to follow development of the failure due to its high speed, different patterns can be recognized in the final crack position:

1. Lowest lamella failure in knot section with wide horizontal crack. It can be followed with failure of next lamella in further location.

2. Same, but lowest lamella fails in FJ

3. Failure happens at the location where two knots are situated in the same or adjacent cross-sections. Two lamella act as one unit, which peels off after tension failure of the knot sections.

4. Lowest lamella failure in FJ with FJ in second lamella nearby - question of interaction of finger joints in that situation is the topic for consideration. Larsen (1982) approximates that finger joints interact being closer than five lamella's

Table 1: Beams used for evaluation of model predictions

Source	Beam number	Name	Board class	Lenght, mm	Height, mm	Width, mm	N, kN	f_m, MPa	$E_{m,g}$, MPa	Failure type, 1st lam[1]	Failure type, 2nd lam[1]
Fink et al. (2013)	1	L25-R-1	L25	6000	320	115	74.4	35.6	12'201	knot	FJ
	2	L25-R-2					93	44.5	12'049	knot	FJ
	3	L25-R-3					74.8	35.8	12'006	knot	knot
	4	L25-R-4					69	33	11'312	CW	knot
	5	L25-H-1					59.6	28.5	10'825	knot	CW
	6	L25-H-2					52.4	25.1	10'684	CW	knot
	7	L25-H-3					67.8	32.5	11'768	CW	knot
	8	L25-H-4					71.4	34.2	11'028	knot	FJ
	9	L25-IH-1					77	36.9	11'431	knot	knot
	10	L25-IH-2					69.6	33.3	11'124	knot	CW
	11	L25-IH-3					57.6	27.6	11'694	knot	knot
	12	L25-IH-4					70.6	33.8	11'348	knot	knot
	13	L40-R-1	L40				109.6	52.5	14'896	knot	FJ
	14	L40-R-2					106.6	51.1	15'441	knot	CW
	15	L40-R-3					94.4	45.2	15'571	FJ	knot
	16	L40-R-4					114.2	54.7	15'910	FJ	FJ
	17	L40-H-1					98.8	47.3	14'463	FJ	knot
	18	L40-H-2					87.6	42	15'822	CW	FJ
	19	L40-H-3					118.6	56.8	14'585	FJ	FJ
	20	L40-H-4					96	46	15'284	FJ	FJ
	21	L40-IH-1					91.2	43.7	15'004	knot	knot
	22	L40-IH-2					84.8	40.6	14'522	knot	CW
	23	L40-IH-3					98.4	47.1	15'741	FJ	knot
	24	L40-IH-4					93	44.5	14'542	knot	knot
Stadelmann (2015)	25	GL24h–11m–1	L25	11400	600	158	155.6	30.2	10'700	knot	CW
	26	GL24h–11m–2					178.7	34.7	11'062	knot	CW
	27	GL24h–11m–3					184.2	35.8	10'337	knot	knot
	28	GL24h–11m–4					152.8	29.7	10'483	knot	CW
	29	GL24h–19m–1		19000	1000	178	273.5	28	10'538	knot	knot
	30	GL24h–19m–2					278.8	28.6	10'268	knot	CW
	31	GL36h–11m–1	L40	11400	600	158	218.7	42.4	14'106	CW	FJ
	32	GL36h–11m–2					214.3	41.6	14'162	CW	knot
	33	GL36h–11m–3					197.8	38.4	13'928	knot	CW
	34	GL36h–11m–4					166.2	32.3	14'563	knot	CW
	35	GL36h–19m–1		19000	1000	178	377.9	38.7	13'349	FJ	knot
	36	GL36h–19m–2					440.4	45.1	13'559	FJ	knot

[1] when lamination fails not locally, at few locations along the beam axis, then failure type denotes as follows: if any fraction of lamination width fails at finger joint, FJ failure is stated; if neither knot nor FJ are there - clear wood failure shown (CW), in other cases failure is marked as knot failure.

thicknesses. Similarly, if knots in case 3 have a small shift relative to each other, they also may interact.

5. Lowest lamella failure in clear wood section or with small knot as a result of major knot in lamella above. Knot above induce stress concentration to the lower lamella which happened to be critical.

6. Crack nucleation near knot due to fiber flow pointed out of the cross-section and that crack fades out, stop spreading further. Beam fails with some of above mentioned patterns, not connected with faded crack location.

Patterns from 1 to 4 were described already in Larsen (1982), whereas the last two is observed in the test from this chapter.

Usually, after initial failure of one or few lowest lamellas, crack propagates nearly horizontally, often in both directions. Next lamella breaks at its weakest point along that crack. Kandler et al. (2018) made an analyze of horizontal cracks at beam failure in five 10-beam samples.

Shear failure is out of the scope of this thesis, but still can be mentioned here. It typically occurs in beam with high h-to-L ratio, notched beams and beams with holes. Usually, crack spans from the area of high shear stress to the beam's end.

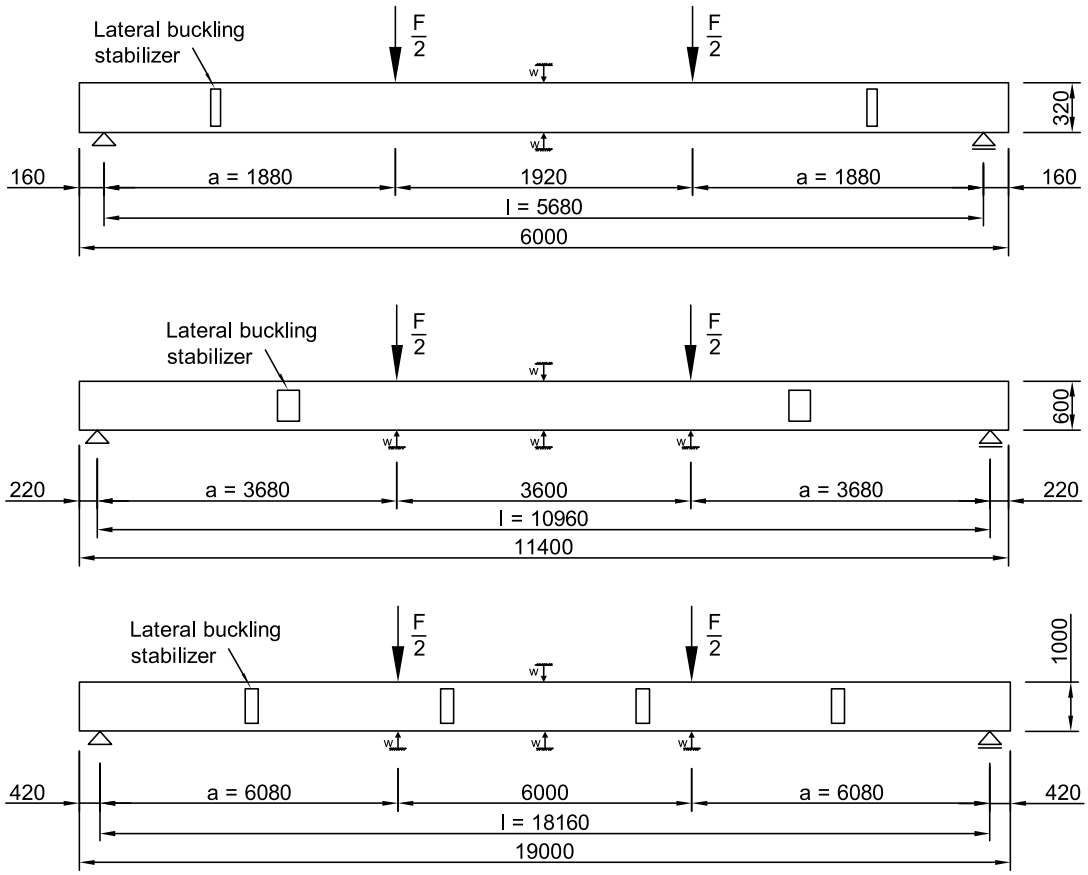

Figure 6: Test setup for beams tested in Fink et al. (2013) and Stadelmann (2015)

4 Material models

In this section, material models for timber properties are discussed. First brief overview of available from literature values and distribution characteristics for every parameter is presented. Then after some discussion the values used in this thesis are given.

4.1 Tensile strength and stiffness along the grain

As was explained before, bending properties of glulam are closely related to tensile properties of its laminations. Precise model for latter is crucial for reliable glulam simulation. Knots and caused by them grain deviation, as well as another defects, cause local reduction of timber strength. High variability of timber is reflected in JCSS probabilistic model code, where coefficient of variation (CoV) for tensile strength of boards is estimated at 0.30 and at 0.13 for the bending MOE.

Two levels of variability of the timber tensile properties can be distinguished. Mean material properties of the entire timber board, and local reduction due to defects, mainly knots. In the thesis model proposed by Fink (2014) was adopted. Taking into account mentioned sources of variability, tension strength and MOE of lamellas he defined using grading indicators E_m and K_m with regression formula

$$\ln(Y) = \beta_0 + \beta_1 E_m + \beta_2 K_m + \epsilon \tag{24}$$

where Y stands for f_t or E of the material cell, β_i is regression coefficients shown in Table 2 and ϵ is normally distributed, zero-centered error term due to stochastic nature of the model. Graphical representation of the dependencies can be found in Fig. 7. According to Fink model, error terms for strength and stiffness are correlated with $\rho = 0.8$. It should be noted that here all the models were done with uncorrelated error terms for simplicity. In Section 5.2.6 and further, modification to the model of Fink is proposed and applied.

Table 2: Parameters for the model to predict E_{WS} and $f_{t,WS}$ based on machine-grading indicators, from Fink (2014)

Model	Parameter	Expected value
E_{WS}	β_0	8.42
	β_1	$7.29 \cdot 10^{-5}$
	β_2	$-1.19 \cdot 10^{-4}$
	σ_ϵ	$9.74 \cdot 10^{-2}$
$f_{t,WS}$	β_0	2.97
	β_1	$7.24 \cdot 10^{-5}$
	β_2	$-2.43 \cdot 10^{-4}$
	σ_ϵ	$1.19 \cdot 10^{-1}$

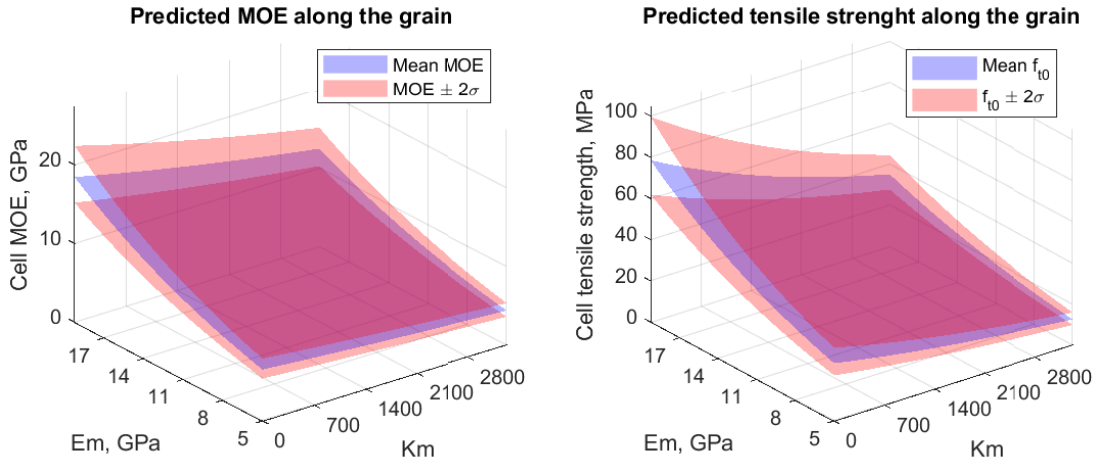

Figure 7: Tensile MOE and tensile strength of lamella based on grading parameters E_m and K_m represented with error term by model of Fink (2014)

4.2 Properties perpendicular to the grain

Weak spot of timber as a material is its low tensile strenght perpendicular to grain, $f_{t,90}$, accompanied by brittle failure mode in this direction. Strength of clear wood perpendicular to grain mentioned in Thelandersson & Larsen (2003) as most commonly found literature value is 3 MPa. Values in range from 1 to 4 MPa also can be met. JCSS suggest to define the strength two-point Weibull distributed with 0.25 CoV value. Also Stuefer (2011) and Brandner & Schickhofer (2014) had tested 150x150 pieces of Central European Norway spruce boards of grade L25 and got mean value of transverse tensile strength 2.7 MPa with CoV 22%. As regrads stiffness perpendicular to the grain, it is also significantly lower than in longitudinal direction. It is commonly considered to have lognormal distribution.

Transverse tensile strength is relevant in post-fracture analysis of glulam, as the initial failure usually happend along the grain. Implementation of material behavior dependency of the strength from overall board properties and local knottiness may be useful for more accurate modeling. Stuefer reported minor negative influence of knots on the $f_{t,90}$. Mean KAR in different samples was from 0.09 to 0.19. Median strength for specimens with knots was 5% lower. Coefficient of determination for $f_{t,90}$ and KAR was -0.18. Correlation of strength with density was not confirmed. Correlation with transversal MOE is weak. This suggests to set $f_{t,90}$ as some function of knottiness. But more studies are required to establish more consistent model.

In current work the main focus is on the bending strength of glulam. Thus extremely simplified approach is chosen to represent tensile strength across the grain. In the only model in the thesis where this parameter is needed, it is taken as 3 MPa for all the material cells. MOE perpendicular to the grain was deducted from JCSS recommendations and taken to be

$$E_{t,90} = E_m/30 \tag{25}$$

where $E_{t,90}$ is modulus of elasticity perpendicular to the grain, E_m is dynamic stiffness of every board obtained with grading device.

4.3 Compression properties

Timber is highly anisotropic material. Futhermore it exhibits different properties in compression and tension. Compressive failure in timber is ductile while tension is brittle. Stiffness properties as well as strenght limits are also not symmetric. Plastic behavior of timber is not adressed in this thesis, but influence of stiffness difference in studied. Dinwoodie (2000) states that MOE in compressive, tensile and bending modes is approximately equal. Whereas from Kin & Shim (2010) compression stiffness is about half of tensile stiffness along the grain for major Korean softwoods of structural size. Correlation coefficient between compressive MOE and tensile was reported 0.879. Fink (2014) in his model presumes clear wood and knot sections exhibit opposite trends regarding compression stiffness in comparison with tensile.

In this thesis, for simplicity, as bending failure of the beam is defined to be tensile rupture of the material, timber was considered as linearly elastic material without compressive strength limit. Two simulations were done to examine influence of compressive MOE, but for the rest of the thesis compressive MOE was taken to be same as tensile one.

4.4 Shear properties

Shear properties of Norway Spruce from few sources are shown in Table 3. JCSS suggest shear strength for softwoods to be a power function of bending strength and have a lognormal distribution. The trend is established only for clear wood specimens. Shear failure is characterized there as brittle.

It would be useful, for prediction of cracking pattern, to be able to better estimate local shear properties for timber. It seems likely that knots, with its grain deviation significantly influence shear strength. Cao et al. (2018) reported 26.2% increase of longitudinal shear strength for Southern Yellow Pine samples with "sound" knots (without decay) situated perpendicular to shear plane, and 9.6% increase for those parallel to shear plane. Knots with decay lower shear strength by 7.6% and 14.4% correspondingly. Assuming properties of softwoods to be similar, and that during grading and lamella composition processes decayed knots was eliminated, shear strength could be modeled positively correlated with knottiness. Yet, more investigations are needed to establish reliable model in regard to knot influence on the shear strength.

For FEM models in the thesis shear modulus G_v is taken from recommendations

Table 3: Shear properties of Norway spruce along the grain. CoV is shown in the brackets

	G_{LR}, MPa	G_{LT}, MPa	$f_{v,LR}$, MPa
Dahl & Malo (2009*a*), (2009*b*)	641(0.24)	582(0.37)	6.1(0.21)
Müller et al. (2004)	541(0.20)		5.5(0.25)
Dinwoodie (2000)			9.8(0.14)

of JCSS lognormally distributed as fraction of tensile MOE:

$$G_v = E_m/16 \tag{26}$$

Shear strength, in the absence of well established model, is taken as constant value 3.5 MPa for the whole beam. Following the example of Serrano & Larsen (1999), value of poisson ratio is taken as 0.45.

4.5 Fracture properties

Fracture energy of the material may have influence to the load-bearing capacity of the simulated beams when propagating fracture is considered. To use Hashin's damage model for 2D problem in Abaqus fracture energy along and across the grain should be provided.

Unfortunately, JCSS doesn't yet give any recommendations about fracture energies for timber to use in the modeling. However there are numerous studies about cracks which develops along the grain. As is seen from tests, in bending, after breakage of lower one or few lamellas, layers of thickness 25-40 mm and more delaminates and horisontal cracks spread. In these cracks, according to Serrano & Larsen (1999), some mixture of modes I and II takes place. In the article authors took fracture energy for cracks along the grain as $G_I = 360J/m^2$, $G_{II} = 980J/m^2$. In the model presented in the thesis intermediate value for fracture energy along the grain of $G = 500J/m^2$ was used to account for mode mixture.

Measuring fracture energy across the grain (LR or LT system) is not a trivial task, because crack tends to kink and propagate along the grain independently from initial notch direction. Schniewind & Centeno (1973) reported LR and LT fracture energy for clear Douglas Fir to be 7-8 times higher than in other systems (2.5 against $0.35MN \cdot m^{-3/2}$). Conrad et al. (2003) after reviewing fracture literature of solid wood conclude as well that fracture toughness perpendicular to the grain is approximately one order of magnitude greater than for parallel to the grain cracks. Stress intensity factor for across the grain cracks is reported in Prokopski (1996) as $K_{I,c} = 2.306MN \cdot m^{-3/2}$ for pine with MC 12%, CoV = 19%. In report of Larsen & Gustafsson (1990) critical fracture energy perpendicular to the grain, mode I, was found to be positively correlated with density, when samples of different European softwoods was treated as one population, with correlation coefficient of 0.78. Correlation reported inside the species was small. Checks and other defects reduce the strength and fracture toughness of the material, but Conrad et al. (2003) expect knots to increase the fracture toughness of timber.

Deterministic value of fracture energy across the grain $5310J/m^2$, which corresponds to values published in Prokopski (1996) was used here in the GLT FE model. However in future for use in Monte-Carlo simulation, it would be interesting to use probabilistic representation of fracture energy taking into account the knottiness influence.

4.6 Properties of finger joints

Strength properties of finger joints (FJ) significantly affect glulam beam strength. Thelandersson & Larsen points out that 40-60% of the beams with FJ in the maximum stress area failed at FJ. In the thesis two approaches to strength of FJ are examined. First one is described in Fink (2014) and strength of FJ is as of the knot section with certain KAR value. That equivalent KAR value can be taken to closely represent strength reduction in FJ corresponding to quality of FJ of particular FJ manufacturer. Statistics from manufacturer would be needed in that case. Here the K_m value was taken to be 1200. For comparison, second approach defines strength of FJ from its E_m indicator by linear regression formula from research of Stadelmann (2015), Eq (27).

Stiffness properties of FJ is similar to CWS and thus taken as the mean stiffness of adjacent cells (Fink (2014)). The rest of FJ properties was taken same way as for the rest of cells.

$$\ln\left(f_{t,FJ}\right) = 3.052 + 5.11 \cdot 10^{-5} E_m + \epsilon \tag{27}$$

where $f_{t,FJ}$ is tensile strength of FJ cell, ϵ is normally distributed, zero-centered error term. Stadelmann (2015) estimates its standard deviation as $\sigma_\epsilon = 0.16$.

5 GLT models

In this chapter developed models for GLT are presented and its performance is evaluated on the set of full-scale beams. It is examined, how well different models are able to predict strength and stiffness of the beams, and what is the effect of using various material and calculation models. In the beginning, the whole modeling process is outlined. Then two methods with its variations are shown - transformed cross-section and finite element methods, and its results are presented. Conclusions for the methods are in the end of corresponding sections.

5.1 Modelling process

In short, the whole modeling process is described on flowchart in Fig. 8. From tests of Fink et al. (2013) and Stadelmann (2015) local grading indicators E_m and K_m are known for all the boards as well as boards layup. Using material models from previous chapter, corresponding material properties are assigned to all elements of the beam. The term elements here denotes part of the beam with identical mechanical properties. The size of these elements, or cells, corresponds to lamination height in current area of the beam and its length is 50 mm. For more information about properties used, see each model description. In all the models, Monte-Carlo simulation was performed for those tested 36 beams. 100 times for each beam calculation was repeated. In every repetition, or setup, error term in the strength and stiffness regression model was changed in accordance with the corresponding probabilistic model, based on the grading indicators. For models, using identical material models, a random set of error terms was kept the same for better comparability of results. Characteristic features of analyzed models can be found in Table 4. Numeration of models was done in the course of the working process and therefore not perfectly consistent.

Every model, from 1 to 9, consists of 3600 runs of beam simulation. As the amount of needed operations is huge, scripting was widely used. Matlab coding was used for TS simulations. Numerical FEM simulations were run in the Abaqus 2019. To manage FEM models Python scripting under Abaqus environment was exploited. The heaviest numerical simulations, FEM models, were mainly done on the Puhti supercomputer of CSC – IT Center for Science, Finland. An outcome of simulation for every model was collected to separate Matlab data file. Output is unified, so the same Matlab script can postprocess all, TS and FEM, model results. Among other data, every file contains an estimated load-bearing capacity and the location of initial failure in every setup. Based on this data and test results, model performance is evaluated. Compilation of model results is shown in Table 5. Predicted strength distribution is plotted, compared with tested load-bearing capacity, as well as failure location predictions are analyzed. These graphical results are shown in appendices of the thesis.

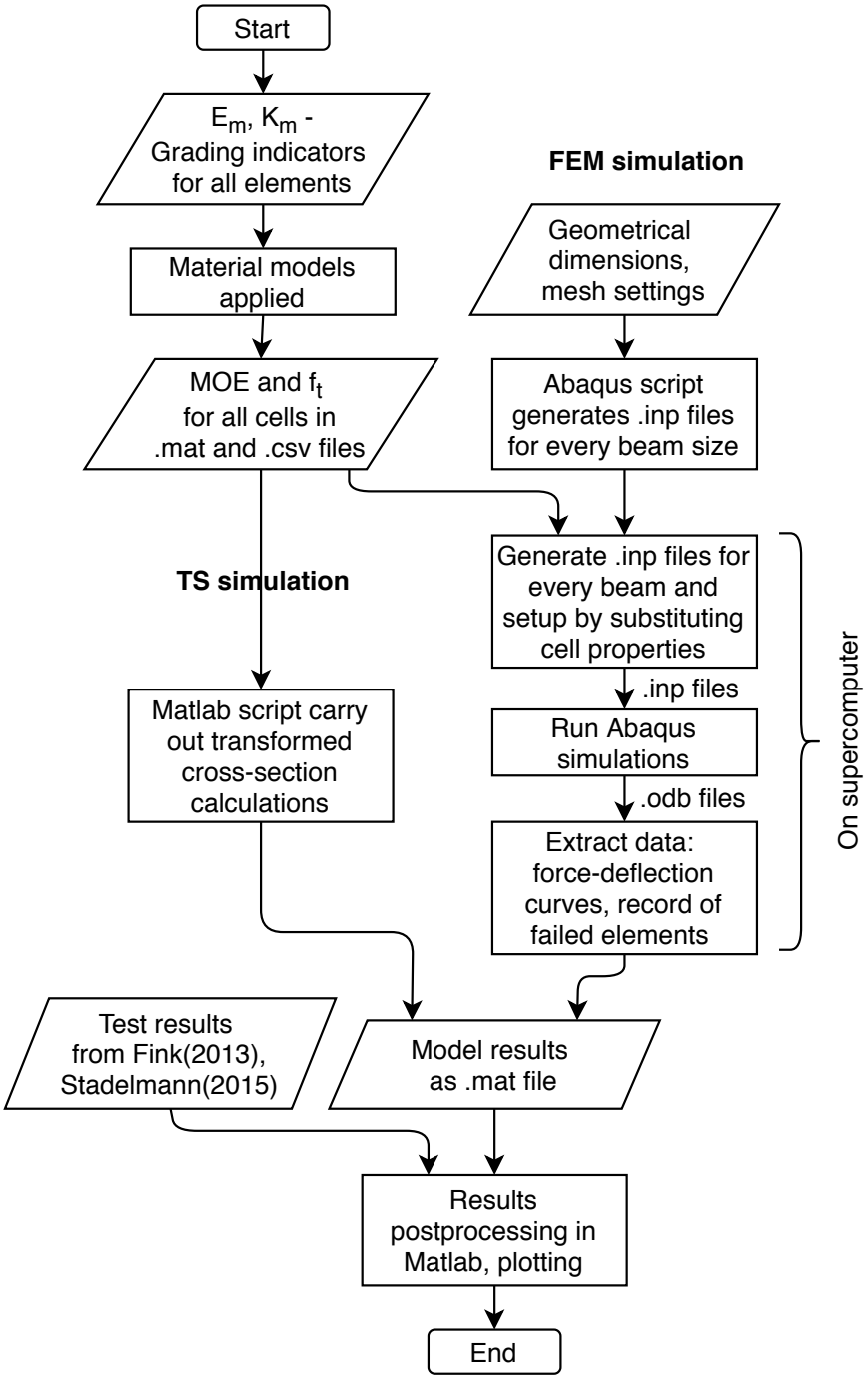

Figure 8: Flowchart for the simulations done in the thesis

Table 4: GLT models done in the thesis

Model	Method	$\beta_{2,ft}$[1], 10^{-4}	Model for FJ[2]	Definition of failure	For FEM		Note
					Mesh[3]	Material	
1	TS	-2,43	F	Load at first element failed	-	-	-
2a							$E_c = 0.8\ E_t$
2b							$E_c = 1.2\ E_t$
2c			S				-
3				Maximum load after 5 failed elements with delamination			
4				Load at first element failed			E = const
4a							Ft = const
4b		-1,73					-
4c		-2,17					
4d		-1,73	F				
5	FEM	-2,43	S	Maximum load from load-deflection curve	1, linear	Isotrop.	-
6						Ortho-tropic	
7					1, quad.		
8		-1,73	F		2, quad.		Not performed
9					5, linear		

[1] Parameter used in the regression model for tensile strength along the grain, Eq. (24). In the model proposed in Fink (2014) the value is $\beta_{2,ft} = -2,43 \cdot 10^{-4}$

[2] Finger joint strength model; F stands for model from Fink (2014), S from Stadelmann (2015)

[3] Mesh size and order; number shows the amount of finite elements per lamination height

5.2 Transformed section method

Outline of the transformed cross-section approach in general was presented in Section 2.2. In this section variations of transformed section model is intoduced and applied to the set of tested beams. In the end of the chapter, conclusions made during TS simulations are summed up.

5.2.1 Basic TS model

In the first transformed cross-section model, material model for strength and stiffness properties of the beam cells from Fink (2014) was used. Tension stress at mid depth of lamina is compared with tensile strength of corresponding element for every

Table 5: Models performance in predicting GLT bending strength. Definitions of the models can be found in Table 4

Model	R-squared of f_m			Mean CoV[1] of f_m, %			Mean error[2] of f_m, MPa		
	All	L25	L40	All	L25	L40	All	L25	L40
1	0.71	0.18	0.38	7.5	8.1	7.0	-2.9	-4.6	-1.3
2a	0.69	0.13	0.35	4.8	5.0	4.6	-0.9	-3.3	1.4
2b	0.72	0.21	0.44	7.8	8.1	7.5	-2.1	-3.7	-0.6
2c	0.68	0.13	0.34	7.8	7.8	7.7	-2.8	-4.2	-1.4
3	0.66	0.14	0.25	6.9	7.1	6.8	-2.3	-3.6	-0.9
4	0.69	0.15	0.35	7.2	7.4	7.1	-7.5	-9.4	-5.6
4a	0.12	0.04	0.23	3.5	3.4	3.5	-2.9	2.5	-8.4
4b	0.75	0.40	0.42	7.2	7.3	7.1	0.0	-0.5	0.5
4c	0.73	0.26	0.44	7.4	7.8	7.1	-1.8	-2.9	-0.8
4d	0.75	0.39	0.42	7.2	7.5	6.9	0.0	-0.8	0.9
5	0.67	0.15	0.26	6.9	7.3	6.5	-2.8	-4.4	-1.3
6	0.68	0.14	0.33	7.3	7.8	6.9	-4.3	-6.0	-2.6
7	0.67	0.13	0.27	7.2	7.6	6.8	-7.1	-8.5	-5.7
8	-	-	-	-	-	-	-	-	-
9	0.70	0.23	0.33	5.6	6.0	5.3	-0.8	-2.0	0.4

[1] Mean CoV shows what is average coefficient of variation among all 36 beams, when 100 simulations are done for each.
[2] Mean error column shows the average, among all 36 beams, deviation of mean of prediction from test result

tensioned material cell in every cross-section. The force at which first element fails is taken as failure load for the whole beam, according adopted simplifying approach. Its true that strength will be slightly underestimated, especially for high beams. The reason this approach is chosen rather than progressive failure recording, is the crack pattern observed in most GLT beam tests. If we take the maximum load among first, let's say, 5 failures, we will get overestimated strength as it will not take into account delamination and exposure of next laminations to high stresses at the bottom of reduced cross-section. Such delamination is taken into account in Model 3 (section 5.2.4).

Results of Monte-Carlo simulations from TS Model 1 is shown on Fig. 9. There predicted probability of bending strength is plotted for every beam, placed on x-axis according to its test bending strength. Kernel density estimation was used to plot the curves from data points of 100 simulations per beam. Beam number according to Table 1 is shown next to each curve. Small dots indicate distributions' means. For comparison of different models graphs in bigger scale is given in Appendix A for beams from boards of grade L25 and L40 separately. Predicted mean stiffness and strength plotted against test result is shown on Fig. 10.

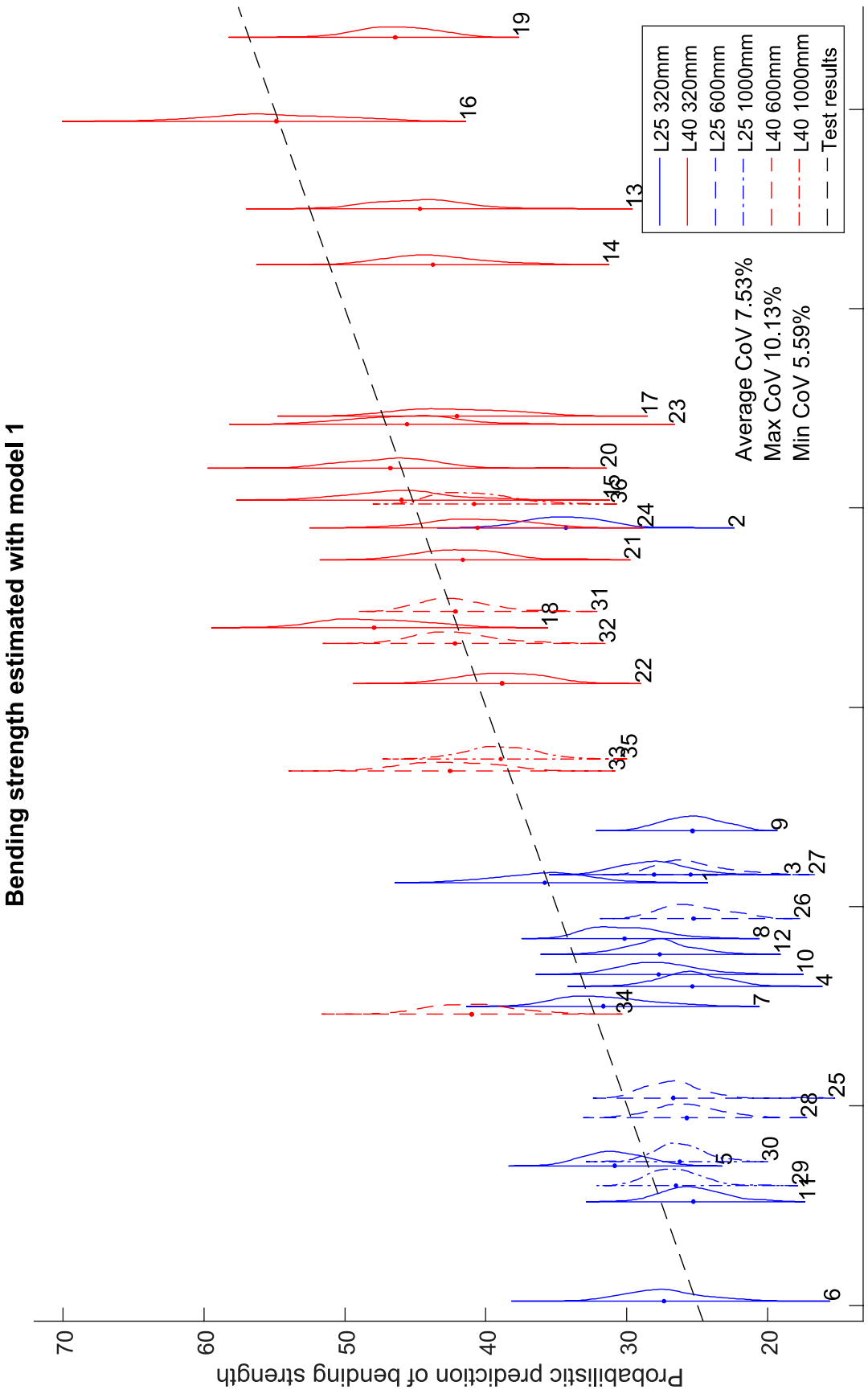

Figure 9: Bending strength distribution by transformed cross-section model

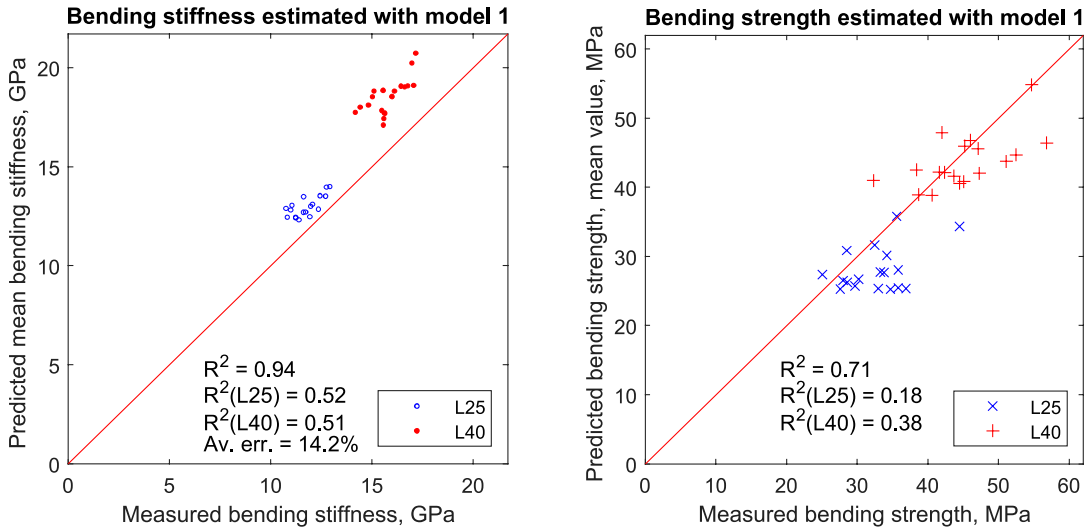

Figure 10: Estimated bending stiffness and strength for all 36 beams computed with transformed section model with material properties according to Fink (2014). Shear stiffness for both test and simulated result is assumed to be 650MPa

Bar plot in Fig. 11 shows what type of cell was at the place where lowest lamella breaks - FJ, knot or clear wood section. For TS model if none of first four failed elements was situated in first lamella, that setup is counted as "failure in upper lamellas". For FE method first two frames after failure initiation was monitored. Red stars represent deviation of mean bending strength of the simulation from test result expressed in standard deviations of prediction. Coefficient of variation for every beam is plotted in the lower part of figure. Plots for the other models are shown in Appendix B.

5.2.2 Influence of compressive stiffness

As shown in Section 4.3, timber may exhibit lesser stiffness in compression than in tension. Simulations 2a and 2b was done to see how this can influence to the mechanical behavior of the beam. Compressed elements were assigned stiffness 20% smaller (Model 2a) or bigger (Model 2b) than their hypotetical tensile stiffness. MOE was assigned to cells in iterative manner. If neutral axis is significantly displaced from the middle of the cross-section, stiffness will be reassigned to the elements that change sign.

Changing compressive stiffness by 20% gives -10,5% and 9,4% change to the beam stiffness correspondingly. In comparison with previous model, model 2a, with lower compressive stiffness, gives higher values of strength. Neutral axis is situated lower, distance from it to the lowest lamella is smaller and this seems to be the reason of higher beam strength. Althought it is not clear then, why simulation 2b doesn't show similar trend with opposite sign. Also author can't explain why CoV in simulation 2a is so low.

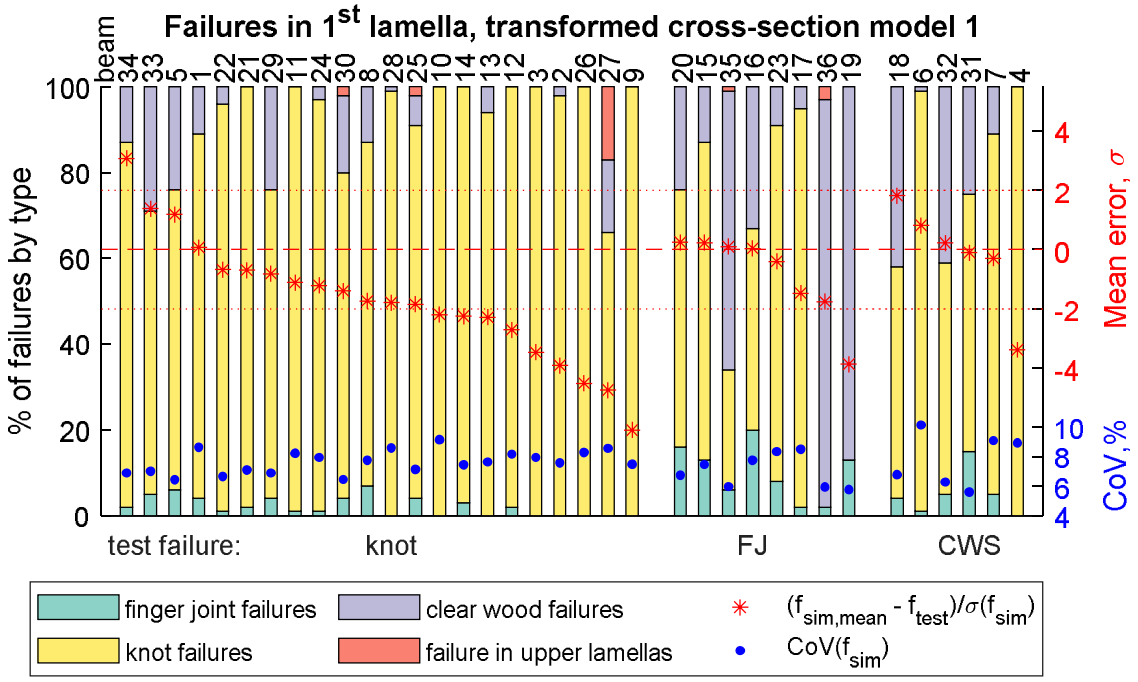

Figure 11: Location of predicted failure in the first lamella predicted with transformed cross-section Model 1

5.2.3 Influence of the finger joint strength model

Model 2c, together with Model 1, allows to compare performance of two considered finger joint strength models (Section 4.6). The difference between Models 4b and 4d is, as well, only in adopted FJ model.

Simulations 1 and 2c, 4b and 4d, with different FJ models, show very similar results concerning the load-bearing capacity of the beams. They exhibit only minor differences in distribution of predicted failure types.

5.2.4 TS model with delamination

As was mentioned in section 5.2.1, after failure of first lamella delamination exposes significant length of the second lamella to higher stresses, not only those above failed element. Thus the probability to have low-strength element there is increased. Petersson (1992), from fracture mechanics considerations, gave formula for estimation of the minimum moment M_c in the beam, causing lowest layer delamination in the presence of the perpendicular to the axis notch or crack, Eq. (28).

$$M_c = \sqrt{\frac{2bG_c}{\frac{1}{E}\left(\frac{1}{I_1} - \frac{1}{I}\right)}} \tag{28}$$

where b is beams width, G_c is critical fracture energy in corresponding mode, I and I_1 is moment of inertia of full and remaining uncracked beam cross-section correspondingly. To simulate delamination effect, Model 3 is done. There, after

element fails in lowest lamination, the whole lamination where bending moment is bigger than M_c is removed from calculation. Critical moment for removal depends on material and the lamination thickness. If first element fails not in the lowest lamella, it is just removed, no delamination happens. The load-bearing capacity of the beam is defined as maximum load-bearing capacity reached until first five elements fails.

Delamination failure criteria did not perform any better than previously described TS models. Therefore it was not investigated further. Stiffness was not checked here as it should be the same as in the Model 2c.

5.2.5 Influence of strength and stiffness variation to the variation of the simulation

It was interesting, how does difference in stiffness between elements influence the strength prediction. And how does variability in strength definition affect it. To investigate these questions Models 4 and 4a were done. In Model 4 everything is as before, in Model 2c, but stiffness of all the elements is the same, 12000 MPa. Model 4a is identical to Model 2c, except that strength of all the cells is constant, 40 MPa. Graphs for bending strength distribution for these models can be found in Appendix, Fig. A3, A4.

Coefficient of determination and CoV of the Model 4 are about the same as were with the Model 2c (Table 5). The main difference is that this artificial model on average underestimates the GLT strength. For lower grade beams underestimation is 5.2%, for higher 4.2%. Lamination effect, mainly "reinforcement of defects" part of it, easily explains that difference. Even when we do not account for relative stiffness difference between elements, the method gives reasonable prediction.

Tensile strength of the laminations is one of the most important input parameters. It is seen from Model 4a: if inherent strength of the cells is not accounted for, model is not able to represent real beam's strength; R-squared for this simulation is 0.12. Model 4a demonstrates that TS method is sensitive to the size of the beam. Beams of height 600 mm and 1000 mm has a noticeably lower strength predicted. It cannot be explained only by the relative position of the calculation point to the bottom of the beam. The reason of such a behavior is not clear for us. From these two models, 4 and 4a, conclusion can be made that influence of the strength variability dominates over the stiffness influence.

5.2.6 Modification for material properties to account for laminating effect

Strength of the beams with knot failures is mostly underestimated. Strength of beams made of lower-class boards are more underestimated then of those from higher class. We assume that influence of the knot on the lamella strength is overestimated and described underestimation can be explained by lamination effect (see section 2.1). It the models, grading parameters from real beams were used in regression model, which is based on lamination tension tests. Transformed section simulation, being run with that regression model, account already for the dispersion effect. It partly model reinforcing effect; stress redistribution considered inside the cross-sections.

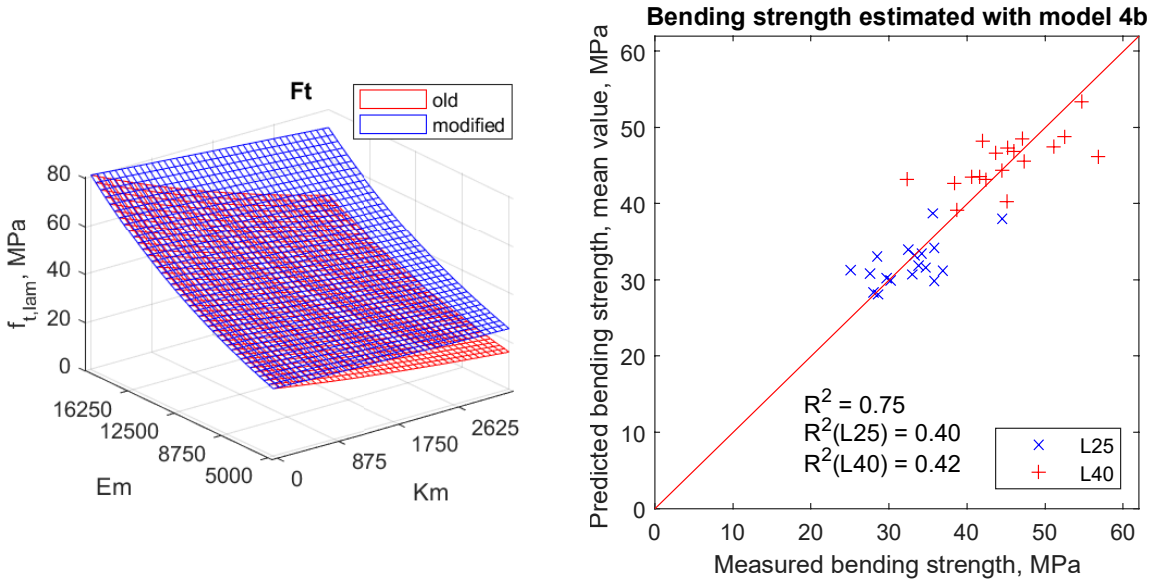

Figure 12: (Left) Modification of tensile strength model; (right) mean strength predicted with transformed-cross section model with modified tensile strength model against test results

However nor TS nor FEM model are not able to incorporate any test procedure effect. This test procedure effect is attempted to be accounted for in this section by modifying the tension strength regression model.

Falk & Colling (1995) represents lamination factor as

$$k_{lam} = k_{test} \cdot k_{reinf} \cdot k_{disp} \tag{29}$$

with k_{test}, k_{reinf} and k_{disp} corresponds to test, reinforcement and dispersion effects. Colling & Falk (1993) estimate k_{test} on the mean level to be from 1.04 for higher strength grade to 1.14 for lower one considered. This was taken as starting point. According to Fink (2014) expected value of tKAR for grade L25 lamellas $E(tKAR_{L25}) = 0.240$ and $E(tKAR_{L40}) = 0.192$ for grade L40. That corresponds approximately to K_m values of 1850 and 1500. To reduce effect of knottiness, parameter $\beta_{2,ft}$ should be adjusted. In Model 4b, 4d and 9 regression model was changed so that for L25 beams cells with $E(tKAR_{L25})$ were 1.14 times stronger ($k_{test,L25} = 1.14$).

$$\beta_{2,ft} = -1.73 \cdot 10^{-4} \tag{30}$$

was used instead of $\beta_{2,ft} = -2.43 \cdot 10^{-4}$ in original model of Fink. That gives $k_{test,L40} = 1.11$ on the mean level for L40. Graphical representation of model modification is shown on the Fig. 12 (left), prediction of mean bending strength with modified model on the Fig. 12 (right), failure location distribution is presented in Fig. 13. Bending strength distributions for the calibrated model can be found in Appendix A.

As a result of described modification, performance of the model significantly improved, especially for the lower grade beams. Comparing Models 1 with 4d, 2c

with 4b, we see that overall coefficient of determination rose from 0.71 and 0.68 to 0.75 and, what is even better, R-squared inside strength classes increase to 0.40 for L25 and 0.42 for L40. There is a chance that proposed modification is suitable only for current set of beams and overfits the model, but author expects it to be reasonable also for general application.

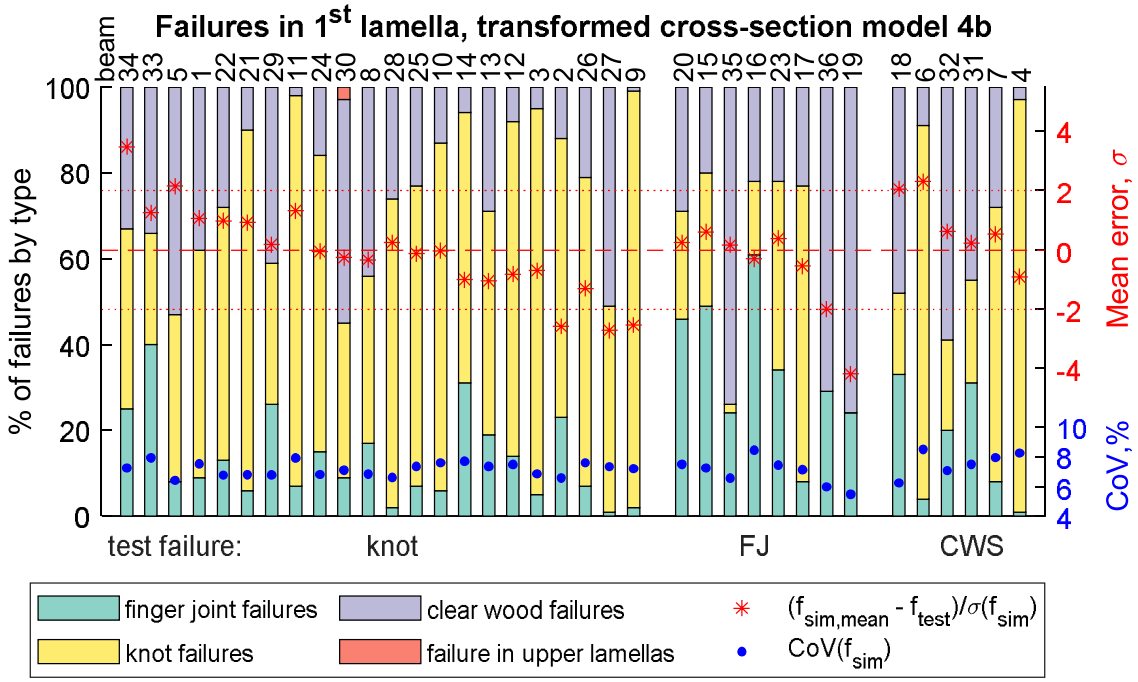

Figure 13: Location of predicted failure in the first lamella predicted with transformed cross-section Model 4b

5.2.7 Summary for transformed cross-section models

Transformed cross section model have provided a tool to briefly estimate beam properties and analyze influence of different model parameters. Main conclusions from applying TS method:

- Setting compression stiffness lower or higher than the tensile stiffness causes beams stiffness to change accordingly. However this modification's influence to the beam strength is not straightforward
- Finger joint strength models proposed by Fink (2014) and Stadelmann (2015) gives similar results in TS simulations
- Progressive failure definition with simulated delamination doesn't improve the model prediction
- Strength properties of the beam cells is key factor for accurate model prediction. Laminating factor due to reinforcement effect, which is emerged from correlation of cells' strength and stiffness, is found to be on average 5%.

– During the course simulations, need for adjusting strength model to account for test procedure effect was revealed. Adjustment improved model performance. Load-bearing capacity of beams was predicted with R^2 of 0.71 with basic material model and of 0.75 with modified one

Using TS method, it is not possible to account for interaction of elements from the neighboring cross-sections, such as closely placed FJ or knots situated in adjacent lamella. Post-fracture behaviour simulated by element deletion barely represent real fracture in the beam.

5.3 Finite element method

Taking into account local material properties of GLT beam, load-bearing capacity and stiffness of the beam can be estimated using a numerical strain-based model (FEM). In this section details of checked Abaqus models are provided as well as the results of Monte-Carlo simulations with these models for the set of tested beams. Influence of meshing to the simulation is evaluated. In the Section 5.3.7 conclusions drawn from the set of FEM models are summarized.

5.3.1 Modeling in Abaqus

In this section the implementation of the finite element model in Abaqus is described. Flowchart for the whole simulation process is shown on Fig. 8. Beams are modeled with 2D elements using plane stress assumption. Geometry of the model is set to be identical to test setups described in section 3, Fig. 14. Different material property is assigned for every 50 mm of every lamella. In Model 9 these cells are further subdivided to smaller finite elements. Elastic material behavior with Hashin Damage model for fiber-reinforced materials is set to the beam elements. Load is applied through rigid load balancer to provide equal forces at both loading point in 4-point bending test. To simulate displacement-driven test conditions, load is applied as displacement at the middle of load-balancer. During the simulation, load-displacement curve is recorded, as well as displacement of midpoint at the bottom of the beam and failure initiation location.

In the tests, to avoid local crushing of wood at support and loading points, pressure is distributed with steel plates. Connection of those plates to load and support points is hinged and allow plates to rotate to be aligned with beam surface when beam deflects. In the model this boundary conditions are modeled by distributing coupling constraints, connecting beam nodes at the "plate" location to hinged reference point

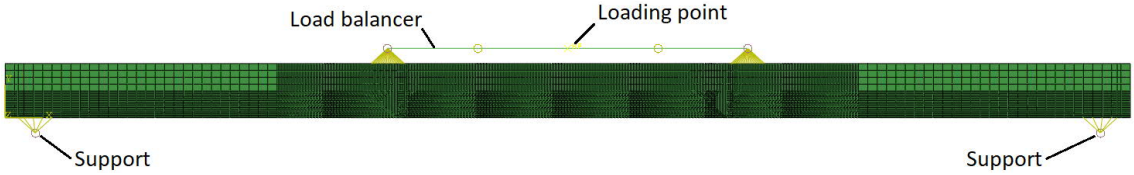

Figure 14: Model of the beam in Abaqus

at the support or load balancer. That doesn't rigidly fix the position of slave nodes between each other, but instead apply forces and moments which resultant is equivalent to those at the master node. This approach helps to avoid singularities near load application area.

5.3.2 Simple isotropic FEM model

At first, the simple finite element model was used. Tensile properties were based on model of Fink (2014). Material had isotropic elastic properties. To stay consistent with definition of tensile strength at the middle of lamella, very sparse mesh was chosen - one linear element with reduced integration per lamella height with length 50mm. Thus stresses were computed at the only integration point in the middle of every element and considered uniform over the whole lamella height. Only longitudinal tensile failure criteria were used by setting very high values for all except fiber tensile strength in Hashin damage model. Fracture energy was set to small value, causing brittle material failure.

Comparison of simple FEM model and transformed section model doesn't show significant difference between these models (Fig. A5, A6). Failure of the beam happens zip-like, i.e. started at some point it develops perpendicular to beam axis until full beam is broken.

5.3.3 Orthotropic FEM model

To evaluate influence of stiffness orthotropy to model behavior, model 6 was established. Model is the same as previous one, except elastic properties are changed to orthotropic. Comparison of isotropic and orthotropic models can be seen in Fig. A7, A8. In result of this change, predicted bending strength decreased for most of the beams and that decrease is more pronounced on beams of lower class. Shape of probability curves barely changed.

5.3.4 FEM model with quadratic elements

Influence of the mesh to the model is a point of interest in this section. Quadratic elements with reduced integration were used in model 7. The rest of parameters are analogous to orthotropic model 6. This meshing implies 4 integration points and linear stress distribution over the element. It leads to the checking failure criteria closer to the most stressed side of the cross-section as well as to higher stress peaks than in case of averaged uniform stress distribution over the element. All that leads to lower load bearing capacities in comparison with model 6, as could be seen from Fig. A9, A10.

5.3.5 FEM model capturing cracking pattern

Timber in general is considered to be brittle material in tension and shear. In general it is assumed that timber strength could be approximated with weakest link theory, i.e. when one element fails, the whole structure fails. Previously presented in that

thesis FE models illustrate that with zipper-like fracture behavior, i.e. when one lamella fails at some location, second fails above it, and so on. Although, due to highly anisotropic and inhomogeneous material properties, under displacement driven loading, formation of first crack not necessary leads to immediate failure of the whole beam. As can be seen from Fink et al. (2013) the remaining after first damage bending strength can be significant. In real glulam after failure of first one or few lamellas, horizontal cracks most often develop. FE model able to simulate that kind of cracking pattern after initial failure is established.

Fracture behavior of material is represented with fictitious crack model. When finite element reach any of the Hashin's failure criteria, instead of crack formation, changing the geometry, remeshing the model and so on, so called "softening" of material is introduced. In reality, while crack opens, stress in the undamaged part reduces from ultimate value to about zero. In the model displacement from crack opening is smeared over the element length. Thus strain increases, stress decreases, so it could be said that material becomes "softer". For detailed description of this approach see, for example, Boström (1992). After failure material properties degrade as described in section 2.5. To reduce influence of the residual stresses in highly degraded elements, when any of finite element's strain reach value 0.04 it is completely removed from the model. Analysis is stopped when reaction force drops by 20% from its maximum (10% for big beams to save computer memory and stay within available resources).

Mesh is denser in the lower lamellas within the area of highest bending moment - five elements per lamination height are used. Mesh horizontal dimension is chosen so to keep elements nearly square in that area. To saves resources mesh is sparse in the rest of the beam. As a drawback, in some setups meshing affects crack development in unnatural way on the border of meshes with different sizes.

Abaqus built-in Hashin damage model for fiber reinforced materials was used. Parameters to define this material behavior include:

- Stiffness properties for orthotropic material. Taken according to Sections 4.1, 4.2
- Tensile strength along the fiber. Tensile strenth is taken according to Fink (2014) approach with modification described in section 5.2. f_t is the function of $\mathrm{E_m}$ and $\mathrm{K_m}$ of every cell with stochastic error term.
- Tensile strength perpendicular to the fiber - tensile strength of timber perpendicular to the grain. For simplicity, here is was taken same for all the elements, $f_{t,90} = 3$ MPa.
- Shear strength along the fiber. Was taken constant, $f_v = 5.5$ MPa. In future it could be taken positively correlated with knottiness.
- Longitudinal tensile fracture energy - fracture energy for cracks in LR, LT systems, cracks crossing the grain. Was taken constant, $G_0 = 5.3$ N/mm.
- Transverse tensile fracture energy - fracture energy for crack along the grain. In simulated glulam beams longitudinal cracks happen under mixed mode. Taken constant, $G_{90} = 0.5$ N/mm

Thus, from material model point of view it is quite simplified model. 2 out of 13 parameters had well established model - tensile strength and stiffness along the

grain. Compressive failure and plastic behavior in compression was not accounted for. Difference in tensile and compressive modulus of elasticity was not considered. In Abaqus user subroutines would be needed to implement that. Some authors mention compressive modulus of elasticity to be 5-10% smaller than tension one. This assumption is slightly supported by the fact that stiffness of the beam predicted with TS method was bigger than in tests.

Results are presented as model 9, in Fig. 15, as well as in Fig. A11, A12 and B6.

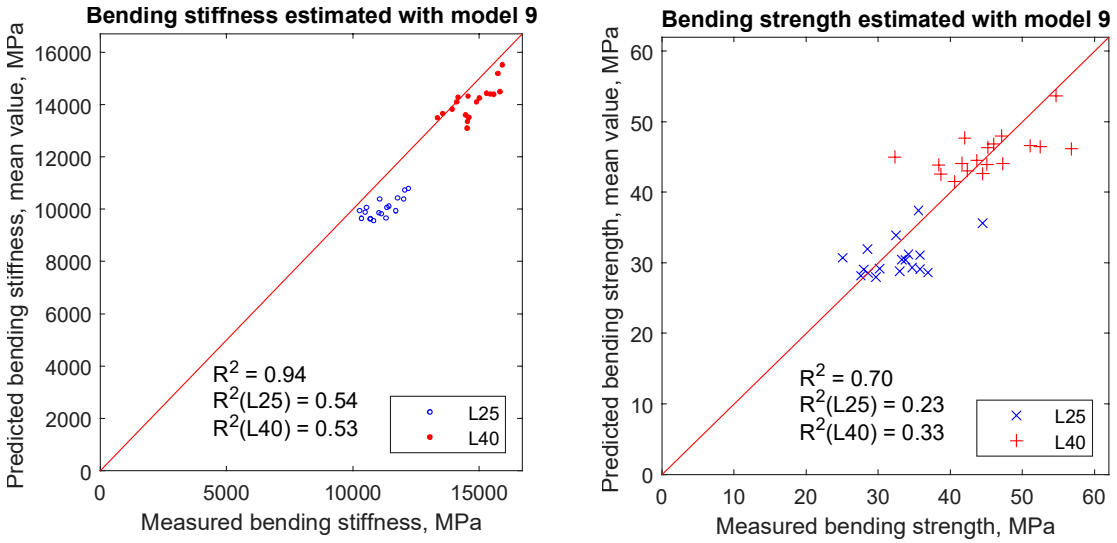

Figure 15: Estimated bending stiffness and strength for all 36 beams computed with FE model against test results

5.3.6 Mesh size influence

Well known that meshing is important in finite element modeling. In the FE model from previous section, failure criterion is checked in the center of every finite element. The smaller elements are, the closer lowest integration point to the most stressed tension side of the beam, the smaller predicted strength is expected. Linear elements, used in the model, average stress over the whole element. With smaller elements, stress peaks are more pronounced, stress distribution and post-fracture behavior is different. Failure criteria in that case could be reached faster.

To investigate influence of mesh size, beams with the same properties but different mesh sizes was evaluated using model described in section 5.3.5 (model 9). Some 4 beams was taken to grasp the trend. Plot is shown in Fig. 16, example of the cracking patterns with mesh sizes from 1 to 6 is shown in Fig. 17.

Simulations converged in all checked setups with mesh size not more than with 6 elements per lamination. For beam of 600 mm height threshold was 4 elements per lamination. Load bearing capacity predicted by the model with mesh sizes of 3 to 5 elements per lamination doesn't exhibit stable trend. For beams 7 and 20 increase of load-bearing capacity at this mesh sizes was accompanied by observed difference in cracking pattern - thickness of delaminating layers was bigger at mesh sizes 1-5 than

at 6-8. For beam 13, initial failure location was changing with different mesh sizes. In presented model mesh size affects cracking pattern and thus ultimate load prediction. For this model, for stable result mesh density of 6 elements per lamination is good.

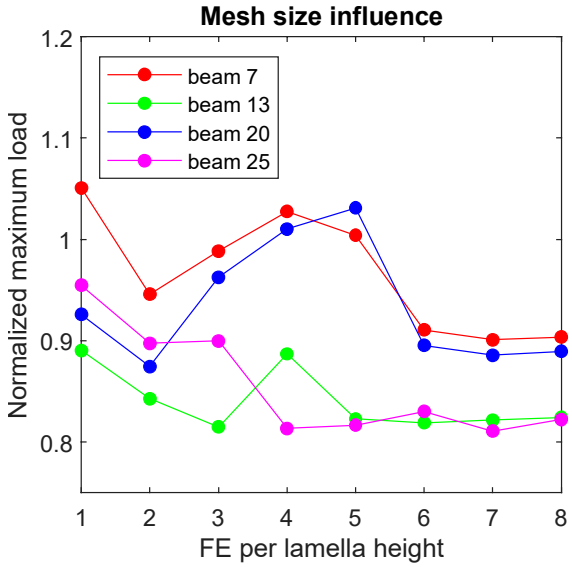

Figure 16: Influence of the mesh size. Normalized load shown is the maximum load in the simulation divided by maximum test load for the beam.

5.3.7 Summary for FEM models

Simplest FEM model gives very similar predictions as transformed cross-section model. Introduction of orthotropy make model underestimate beam load-bearing capacity. Quadratic elements look to be less suitable for use with the simple FEM model, leading to large underestimation of the beam strength.

Preciseness of prediction with FEM agree with work of Colling (1990), where R^2 was found to be 0.70. More complicated FEM model predict strength a bit better than simple one, R^2 is 0.70 against 0.67 for simple model. Although it can be mainly an effect of adjustments for test procedure effect. FEM prediction is worse than one of TS model ($R^2_{TS} = 0.75$). Coefficient of variation of strength prediction with FEM model is on average smaller than for TS models (6.9% for simple one, 5.6% for model 9 against 7.2-7.5% for TS). Coefficient of variation for beams made of higher-class boards is smaller than for lower-class. Not much attention was paid to stiffness prediction in this work. What can be said is that stiffness looks to be underestimated with FEM model.

In addition to load bearing capacity and stiffness, Model 9, described in Section 5.3.5, was able to simulate post-fracture behavior and estimate fracture pattern of the beam. As an example, force-displacement curve from analysis performed all the way to the complete loss of the load bearing capacity is shown in Fig. 18.

For most of the beams, force-displacement diagram look like those shown in Fig. 19 (left). Simulation is stopped when load drops significantly. Although for some

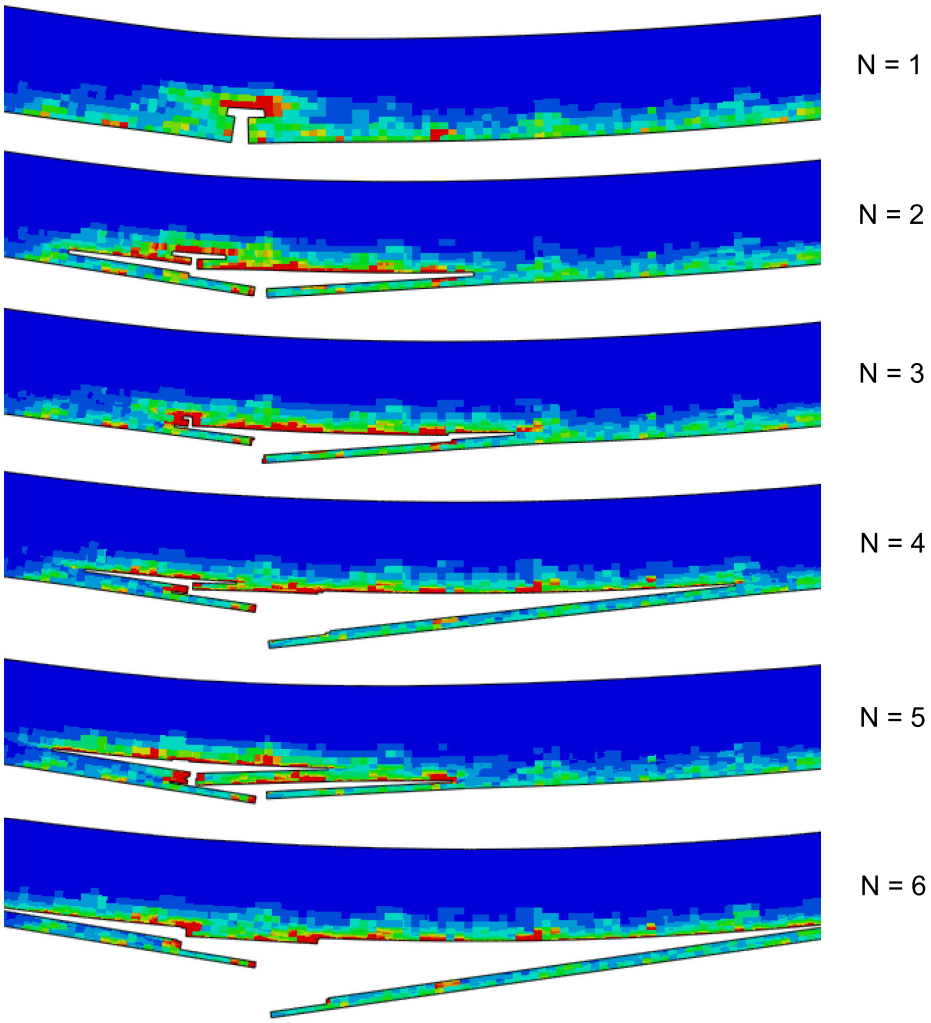

Figure 17: Beam 25 simulated with different mesh sizes. Beam region between loading points is shown. N is the amount of finite elements per lamination height. Colors represent Hashin's tensile failure criteria

setups of beams 28, 29, 31, 34 and 35 maximum load was recorded after first damage. Example is shown in Fig. 19 (right).

Using fictitious crack model with regular square mesh looks to be applicable for predicting cracking behavior of timber beams in bending. After crack across the lamination, shear and tensile perpendicular-to-grain stresses at the crack's corners cause formation of the horizontal crack, like it is observed in tests. The method works fine as the maximum stress area stays at the crack plane. In other loading conditions the model does not represent real cracking behavior correctly: few simulations of high beam with predominate shear failure as well as of beam with hole in maximum shear area was done. There predicted crack was not following grain direction as it does in reality but spreading rather perpendicular to the main tensile stress.

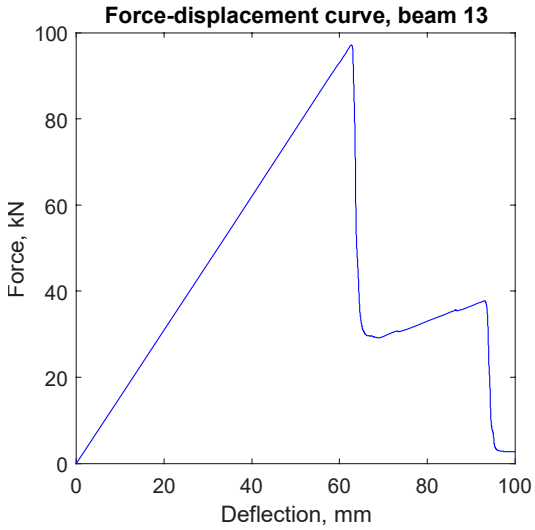

Figure 18: Example of force-displacement curve from FEM simulation capturing post-fracture behavior. The FEM model is described in 5.3.5.

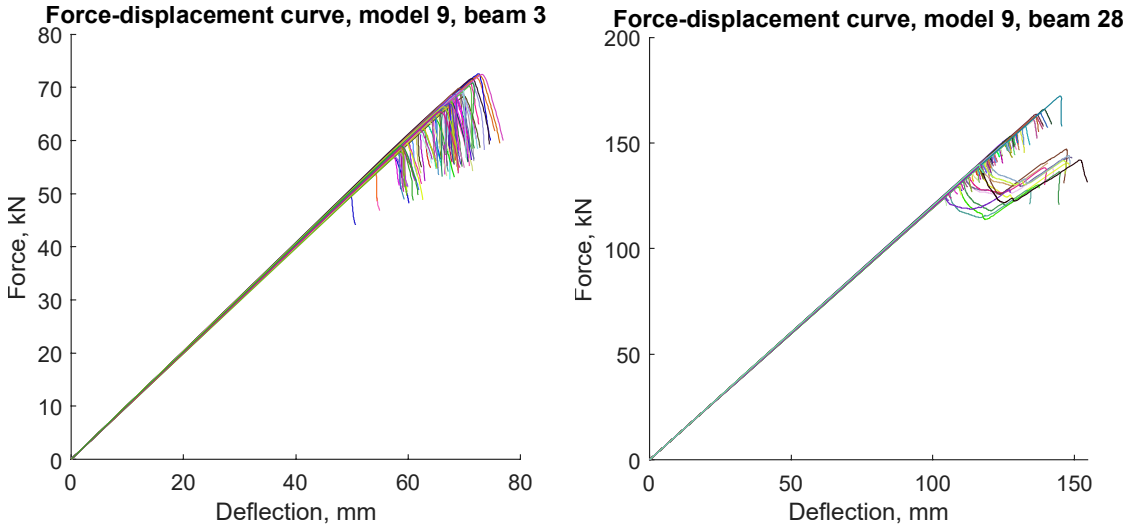

Figure 19: Force-displacement curves of one hundred FEM simulations for two beams. The FEM model is described in 5.3.5. Curves are plotted up to maximum load plus 30 calculation frames or to the last converged frame.

6 Conclusion

In the present thesis different ways to estimate strength and stiffness of glulam beams with well-known local material properties was investigated. Variations of transformed cross-section (TS) and finite element (FEM) models were evaluated on the sample of 36 tested beams. Two types of beams was distinguished: made of class L25 and L40 boards. TS method was used to compare performance of different material models. The purpose of FEM model was not only to simulate strength of the beams, but also estimate the cracking pattern in glulam. Main attention was paid to the strenght properties prediction for the beams rather than stiffness properties.

TS simulation with strength and stiffness probabilistic material model from Fink (2014) was run. It noticeably underestimates the strenght of lower grade beams, showing the need to account for test procedure effect while using Fink's model. After such modifications were introduced, TS model was able to predict load-bearing capacity of the tested beams with coefficient of determination of 0.75 for the whole set and 0.40 for strength classes separately.

Experiments with TS models show that accounting for only tensile strenght of the boards is able to provide prediction with R-squared of 0.69 for both beam classes together. In that case strength is underestimated. Accounting for local stiffness variation, in addition to the strength, improved strength prediction for GLT by about 5%, what gives estimation for laminating factor due to reinforcement effect k_{reinf} for the considered set of beams.

Two approaches to represent finger joint (FJ) strength were considered: thinking about FJ as the knot of certain size and using regression model based on the board stiffness. No significand difference between them was revealed on examined set of beams.

Then, tested beams were simulated using 2D Abaqus model with elastic material and Hashin's damage model. At first, model with coarse mesh and isotropic material was established. As could be expected, it gave very similar prediction as TS model. The use of orthotropic properties reduced predicted load-bearing capacity of the beams in comparion with isotropic model. Another observation made during the work is that linear finite elements perform better than quadratic ones, when Hashin's failure is exploited in Abaqus.

Model to predict crack propagation at failure of GLT beam was developed. Realistic vertical and branching horisontal cracks, formed at glulam bending failure, were simulated. Its shape in the model is very much dependent on the random fluctuation of material properties used in Monte-Carlo simulation. This model allows to simulate the increase of load after the first failure in the beam, which sometimes takes place in tests. Mesh size study for FEM model was conducted. The beam strengh converges with mesh size six times smaller than lamination height. Meshing affected the cracking pattern and the load-bearing capacity of the beam. When models done in the thesis are compared, using TS method for beam strength estimation in Monte-Carlo simulations looks more justified than FEM calculations in Abaqus as the latter is computationally much heavier and doesn't give a better prediction, at least in the form it was done here.

The modeling is done for straight beams and, as it is, could be inapplicable for curved, notched and other special beam cases. All the calculations are done for standard moisture content and temperature.

Presented FE model contains a lot of material parameters, including strength, stiffness and fracture energies for different material orientations. Accuracy of the prediction is heavily determined by quality of material properties predicted. In further study, more precise and realistic material models could be used - strength and fracture energies could be taken as stochastic variables, with certain probability distribution. More comprehensive studies should be done considering the influence of knots on shear and tensile perpendicular to the grain strength as well as on fracture energies in both orthogonal directions. Knowledge about correlation between model parameters would be also useful.

Resolution of the initial data allows mainly lamella-size phenomena to be modeled. Fracture, when started, broke the whole lamella height as it had constant properties all the way through. Data about more precise position of the knot in the lamella height would made fracture pattern prediction to be closer to reality. Furthermore, the influence of crack arrest on ultimate load would be possible to model. Although for most applications the current resolution seems appropriate.

Used fictitious crack model works gives good crack prediction in bending failure mode but not in shear. For cracking prediction for shear problems another modeling techniques should be developed.

Symbols and abbreviations

Symbols

$\beta_0, \beta_1, \beta_2$	regression coefficients in material models
f_c	compressive stregth of lamination along the grain
f_m	bending strength of glulam
f_t	tensile strength of lamination along the grain
$f_{t,90}$	tensile stregth of lamination perpendicular to the grain
G_0	fracture energy for cracks in LR and LT systems
G_{90}	fracture energy for cracks whose plane is parallel to the grain
ϵ	error term in stochastic material models
k_{lam}	laminating factor
k_{vol}	size effect

Abbreviations

E_m	machine grading indicator - dynamic modulus of elasticity of the lamination
FEM	finite element method
FJ	finger joint
GLT	glued laminated timber
KAR	knot area ratio
K_m	machine grading indicator - knottiness parameter
L	longitudinal direction
LR, LT	designation for cracks whose plane is perpendicular to the grain
LEFM	linear elastic fracture mechanics
MOE	modulus of elasticity
MOR	modulus of resistance
R	radial direction
T	tangential direction
TS	transformed cross-section method

References

Abaqus Manual (2013), 'Abaqus 6.13 analysis user's manual', *SIMULIA, Providence, IR* .

Boström, L. (1992), Method for determination of the softening behaviour of wood and the applicability of a nonlinear fracture mechanics model, PhD thesis, Division of Building Materials.

Brandner, R. & Schickhofer, G. (2008), 'Glued laminated timber in bending: new aspects concerning modelling', *Wood science and technology* **42**(5), 401–425.

Brandner, R. & Schickhofer, G. (2014), 'Spatial correlation of tensile perpendicular to grain properties in norway spruce timber', *Wood science and technology* **48**(2), 337–352.

Cao, Y., Street, J., Mitchell, B., To, F., DuBien, J., Seale, R. D. & Shmulsky, R. (2018), 'Effect of knots on horizontal shear strength in southern yellow pine', *BioResources* **13**(2), 4509–4520.

Colling, F. (1990), 'Tragfähigkeit von biegeträgern aus brettschichtholz in abhängigkeit von den festigkeitsrelevanten einflussgrößen dissertation', *Universität (TH) Karlsruhe* .

Colling, F. & Falk, R. H. (1993), 'Investigation of laminating effects in glued-laminated timber', *proceedings of CIB-W18* .

Conrad, M. P., SMITH, G. D. & FERNLUND, G. (2003), 'Fracture of solid wood: A review of structure and properties at different length scales', *Wood and fiber science* **35**(4), 570–584.

Dahl, K. B. & Malo, K. (2009*a*), 'Linear shear properties of spruce softwood', *Wood science and technology* **43**(5-6), 499–525.

Dahl, K. B. & Malo, K. (2009*b*), 'Nonlinear shear properties of spruce softwood: experimental results', *Wood science and technology* **43**(7-8), 539.

Danielsson, H. (2013), Perpendicular to grain fracture analysis of wooden structural elements-Models and applications, PhD thesis, Lund University.

Dinwoodie, J. M. (2000), *Timber: its nature and behaviour*, CRC Press.

Ehlbeck, J., Colling, F. & Görlacher, R. (1985), 'Einfluß keilgezinkter lamellen auf die biegefestigkeit von brettschichtholzträgern', *Holz als Roh-und Werkstoff* **43**(8), 333–337.

Falk, R. H. & Colling, F. (1995), 'Laminating effects in glued-laminated timber beams', *Journal of structural engineering* **121**(12), 1857–1863.

Fink, G. (2014), Influence of varying material properties on the load-bearing capacity of glued laminated timber, PhD thesis, ETH Zurich.

Fink, G., Kohler, J. & Frangi, A. (2013), 'Bending tests on glued laminated timber beams with well-known material properties: Test report', *IBK Bericht* **350**.

Foschi, R. O. & Barrett, J. D. (1980), 'Glued-laminated beam strength: A model.', *Journal of the Structural Division, American Society of Civil Engineers* **106**(ST8), 1735–1754.

Hashin, Z. (1980), 'Failure criteria for unidirectional fiber composites'.

Hernandez, R., Bender, D. A., Richburg, B. & Kline, K. (1992), 'Probabilistic modeling of glued-laminated timber beams', *Wood and fiber science* **24**(3), 294–306.

Jernkvist, L. O. (2000), On the Fracture Behavior of Softwood, PhD thesis, Luleå University of Technology.

Kandler, G., Lukacevic, M. & Füssl, J. (2018), 'Experimental study on glued laminated timber beams with well-known knot morphology', *European Journal of Wood and Wood Products* **76**(5), 1435–1452.

Kin, K. & Shim, K. (2010), Comparison between tensile and compressive young's modulus of structural size lumber, *in* 'World conference on timber engineering. Riva del Garda, Italy', pp. 20–24.

Larsen, H. (1982), *Strength of glued laminated beams: Tests of beams*, number 8201 *in* 'Aalborg Universitetscenter. Instituttet for Bygningsteknik. Report', Institute of Building Technology and Structural Engineering, Aalborg University.

Larsen, H. & Gustafsson, P. (1990), 'The fracture energy of wood in tension perpendicular to the grain', *Results from a joint testing Project-Aus: Working Comission W18-Timber Structures* pp. 23–19–2.

Müller, U., Sretenovic, A., Gindl, W., Grabner, M., Wimmer, R. & Teischinger, A. (2004), 'Effects of macro-and micro-structural variability on the shear behavior of softwood', *IAWA journal* **25**(2), 231–243.

Petersson, H. (1992), 'On design criteria for tension perpendicular to grain', *Proc. of CIB-W18 Paper* pp. 25–6.

Prokopski, G. (1996), 'Influence of moisture content on fracture toughness of wood', *International Journal of Fracture* **79**, R73–R77.

Schniewind, A. P. & Centeno, J. C. (1973), 'Fracture toughness and duration of load factor i. six principal systems of crack propagation and the duration factor for cracks propagating parallel to grain', *Wood and Fiber Science* **5**(2), 152–159.

Serrano, E. & Gustafsson, P. J. (2006), 'Fracture mechanics in timber engineering–strength analyses of components and joints', *Materials and Structures* **40**, 87–96.

Serrano, E. & Larsen, H. J. (1999), 'Numerical investigations of the laminating effect in laminated beams', *Journal of Structural Engineering* **125**(7), 740–745.

SFS-EN 14081-4 (2009), Timber structures. strength graded structural timber with rectangular cross section. part 4: Machine grading. grading machine settings for machine controlled systems, Technical report, SFS.

SFS-EN 408 (2012), Timber structures. structural timber and glued laminated timber. determination of some physical and mechanical properties, Technical report.

Stadelmann, P. (2015), Experimental investigations to evaluate the load-bearing behaviour of glued laminated timber with well-known beam setup, PhD thesis, Master thesis at ETH Zurich, Switzerland.

Stuefer, A. (2011), 'Einflussparameter auf die querzugfestigkeit von bsh-lamellen'.

Thelandersson, S. & Larsen, H. (2003), *Timber Engineering*, John Wiley & Sons.

A Appendix A - Distributions of bending strength prediction

In appendix A bending strength distribution for different models is presented. Number under every distribution curve denote the beam number, text above the curve - failure type of the lowest lamella.

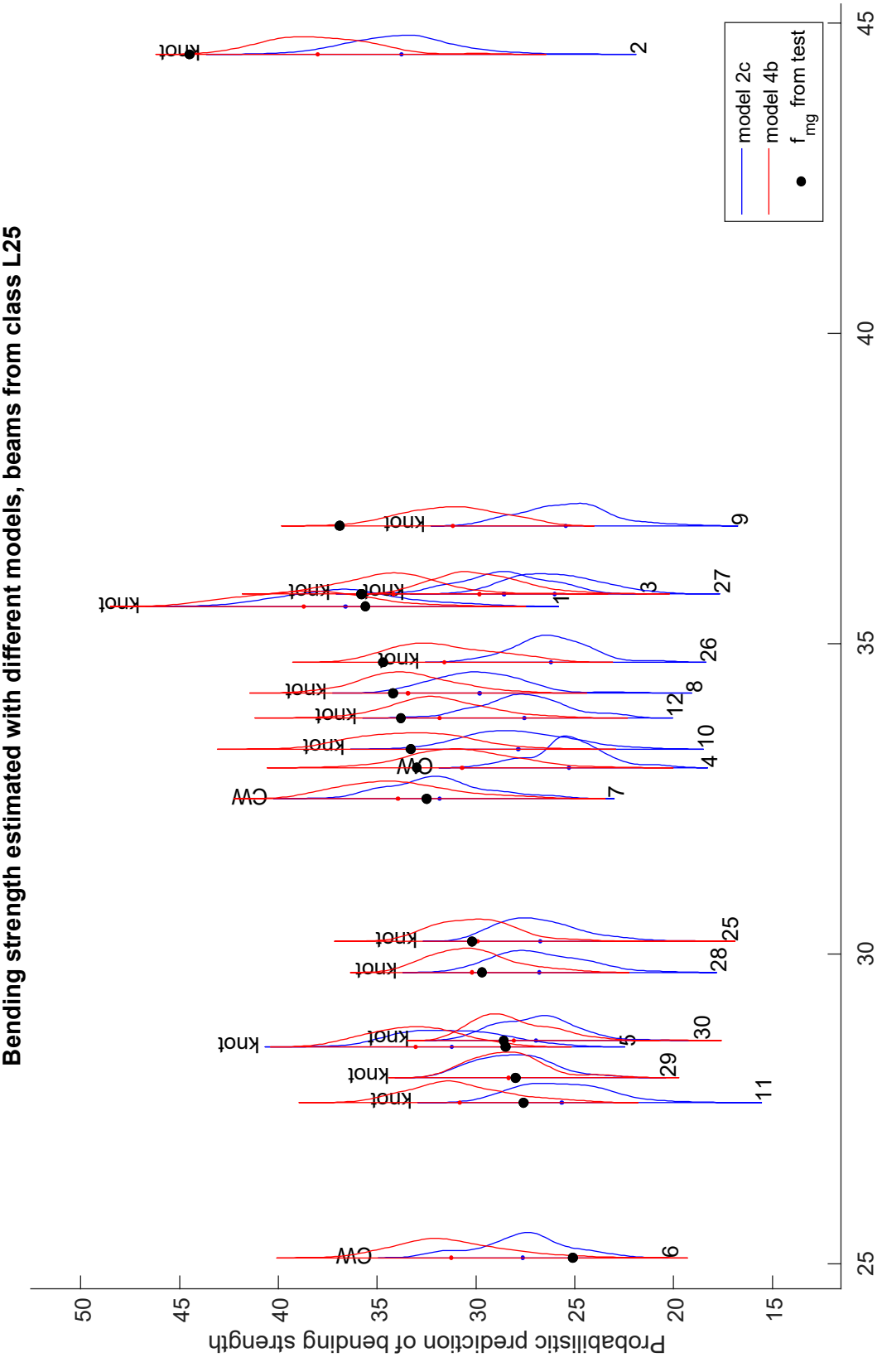

Figure A1: Bending strength distribution for beams made of lumber grade L25. In model 4b strength of knot sections from Fink (2014) model is increased in comparison with model 2c according to Eq. (30). FJ properties from Stadelmann (2015).

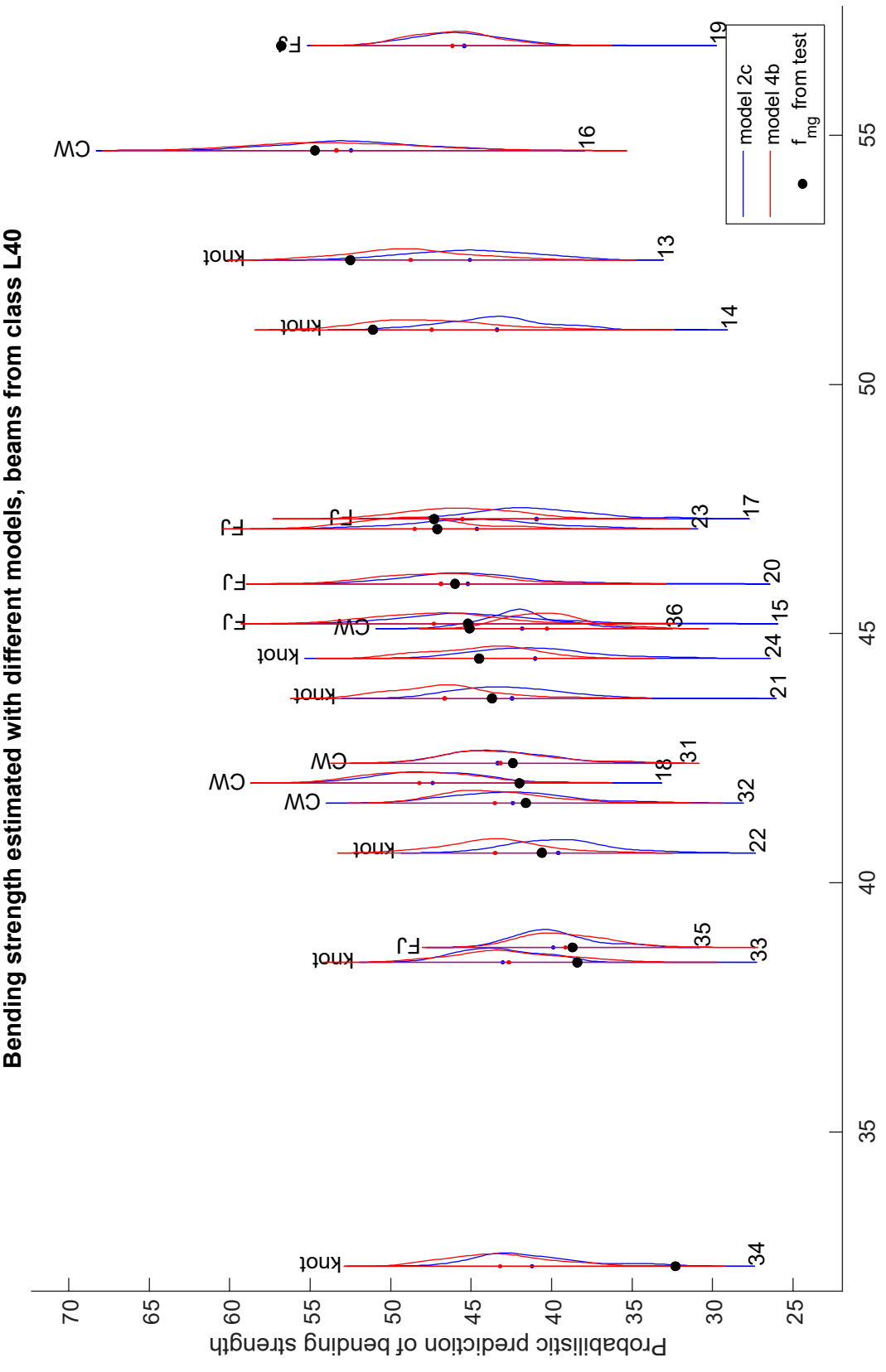

Figure A2: Bending strength distribution for beams made of lumber grade L25. In model 4b strength of knot sections from Fink (2014) model is increased in comparison with model 2c according to Eq. (30). FJ properties from Stadelmann (2015).

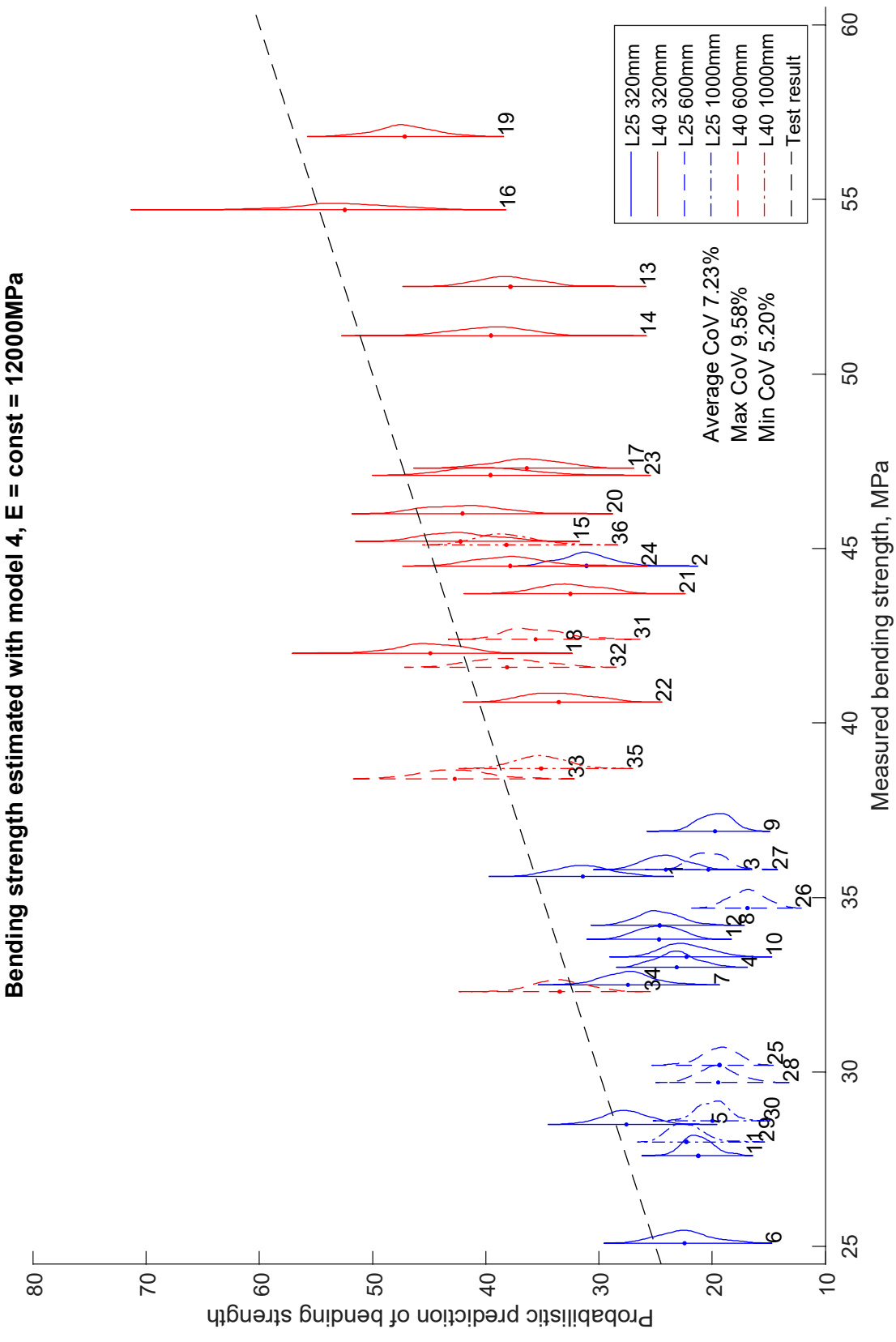

Figure A3: Bending strength distribution calculated with transformed cross-section model when influence of variable stiffness is excluded. Strength of timber according to model from Fink (2014). FJ properties from Stadelmann (2015).

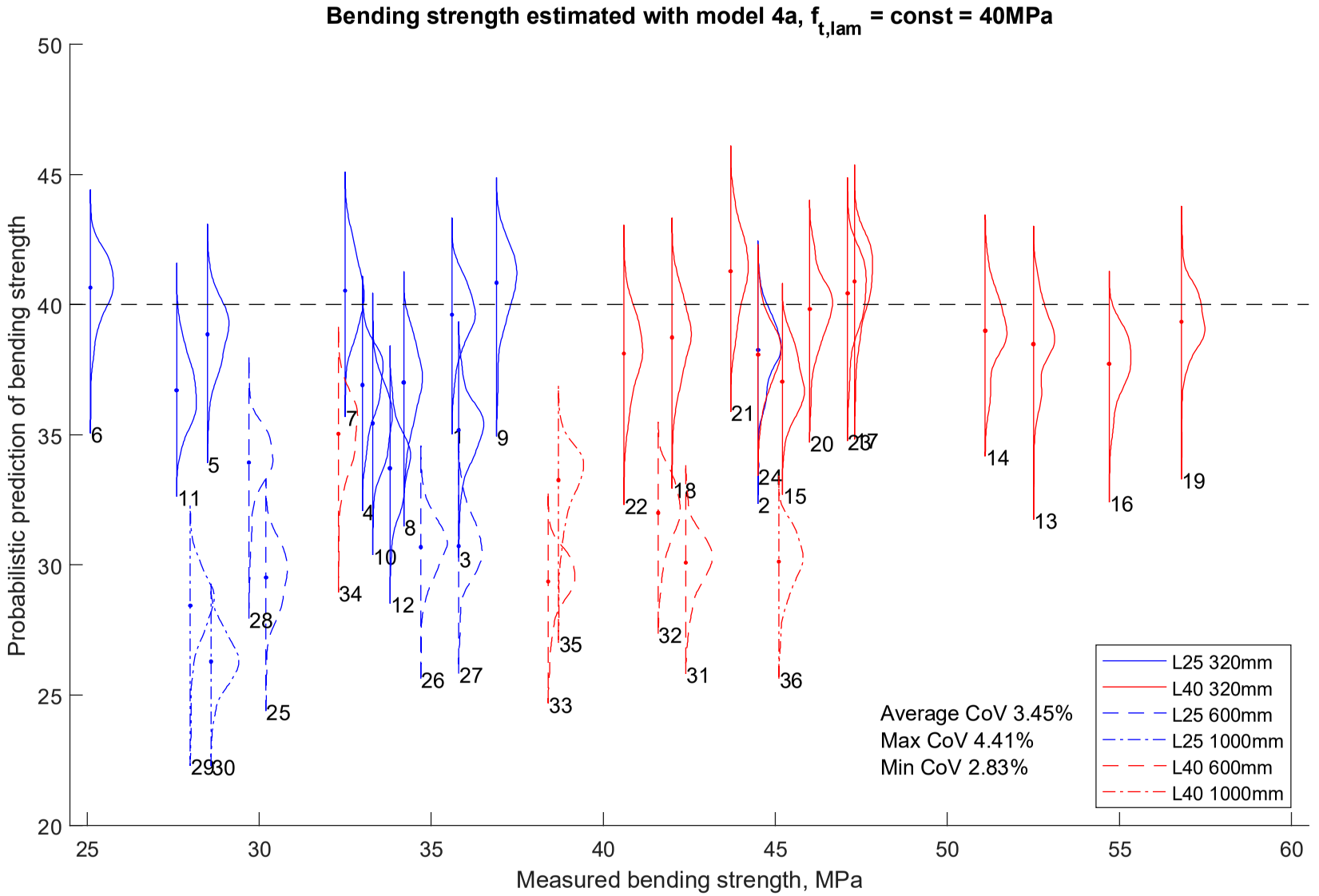

Figure A4: Bending strength distribution calculated with transformed cross-section model when influence of variable strength is excluded. Stiffness of timber according to model from Fink (2014). From Eq. (23) and Eq. (4) $f_{m,g} = \min f_t \cdot \frac{E}{E(y)} \cdot \frac{h}{h-t_{lam}}$.

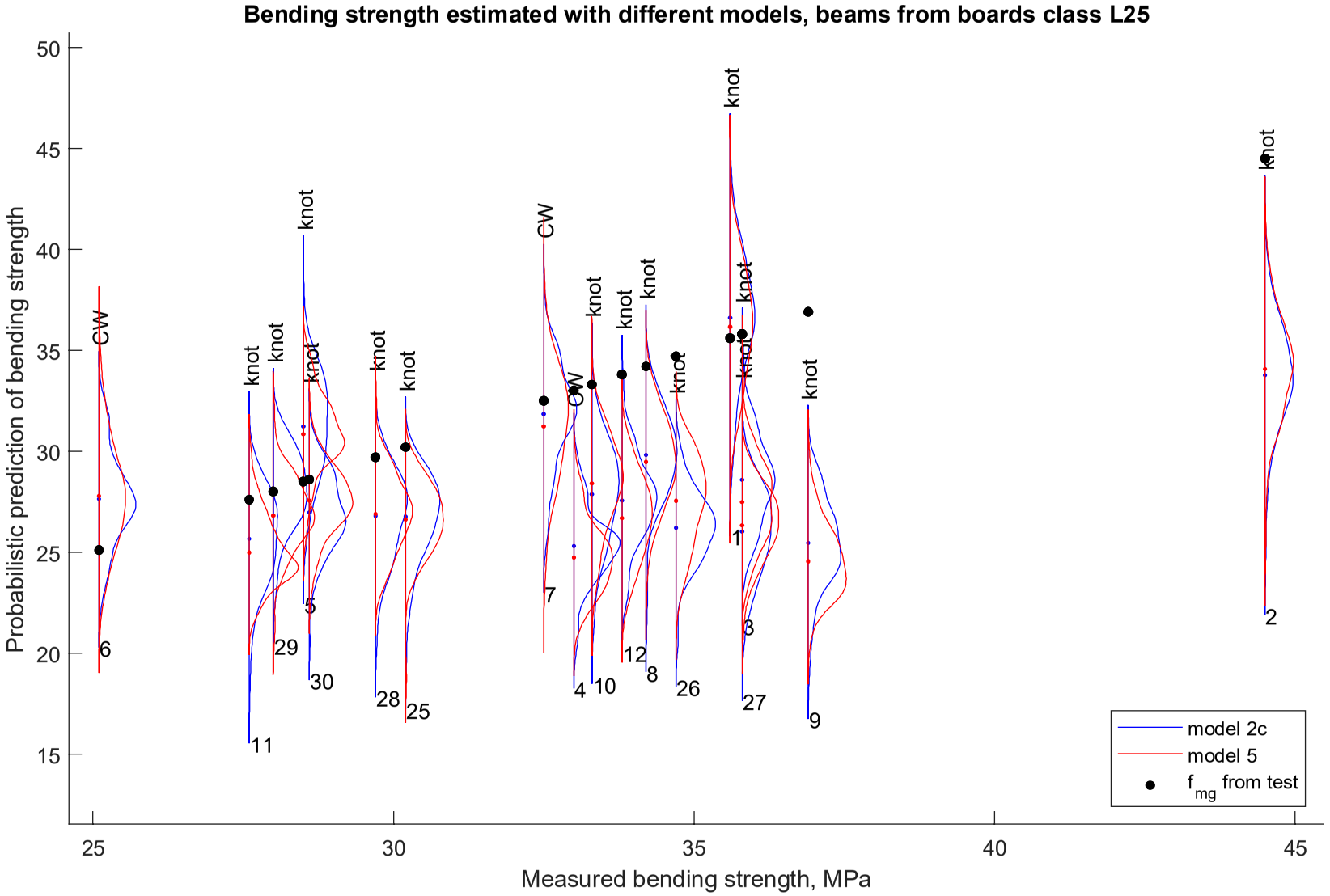

Figure A5: Bending strength distribution for beams made of lumber grade L25. 2c - transformed section model, 5 - finite element analysis, one linear element per lamella.

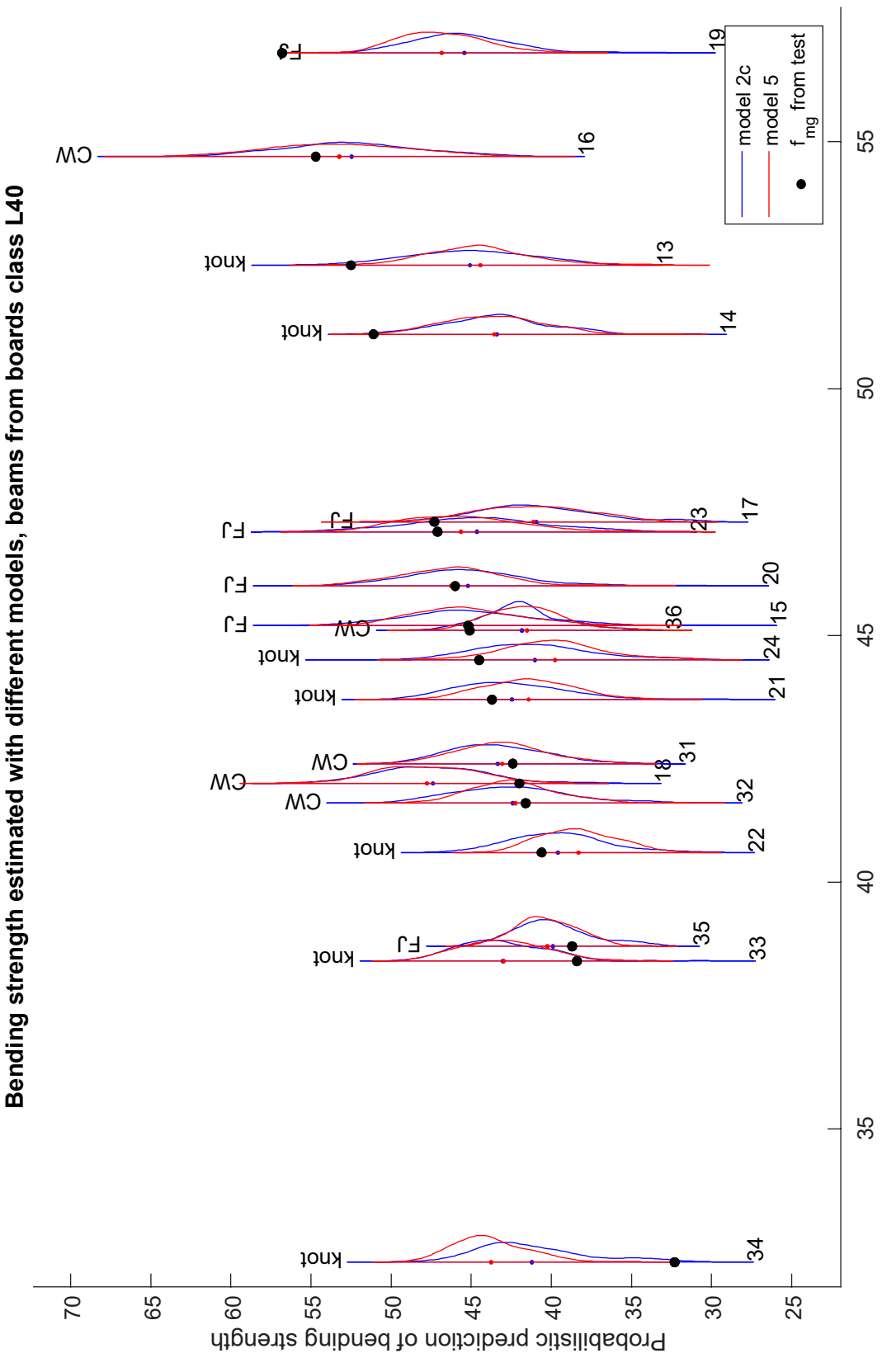

Figure A6: Bending strength distribution for beams made of lumber grade L40. 2c - transformed section model, 5 - finite element analysis, one linear element per lamella.

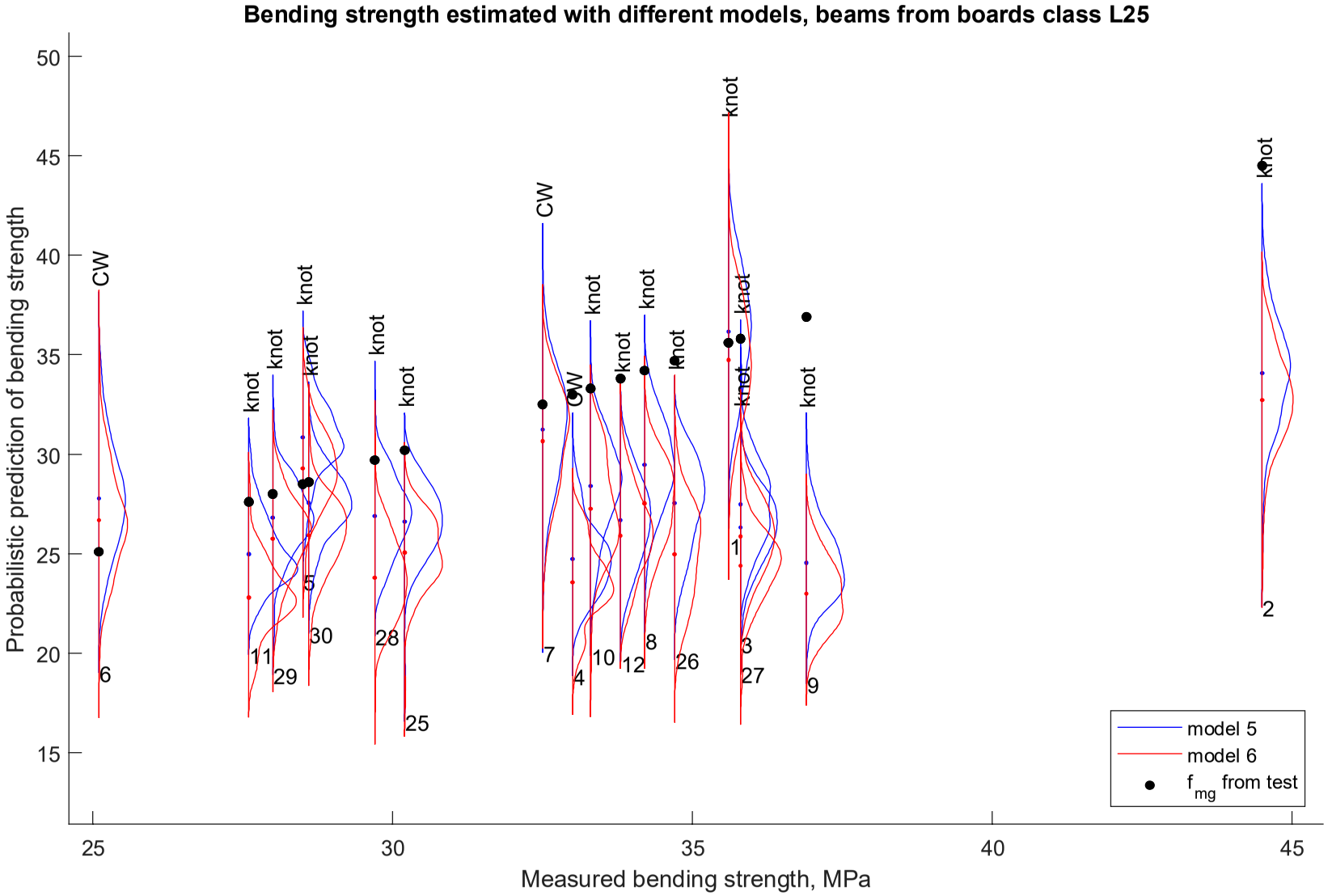

Figure A7: Bending strength distribution for beams made of lumber grade L25 from finite element model, one linear element per lamella, $\sigma_{11} = f_{t,lam}$ as failure criteria. 5 - isotropic material model, 6 - orthotropic with properties from section 4.2. FJ properties from Stadelmann (2015).

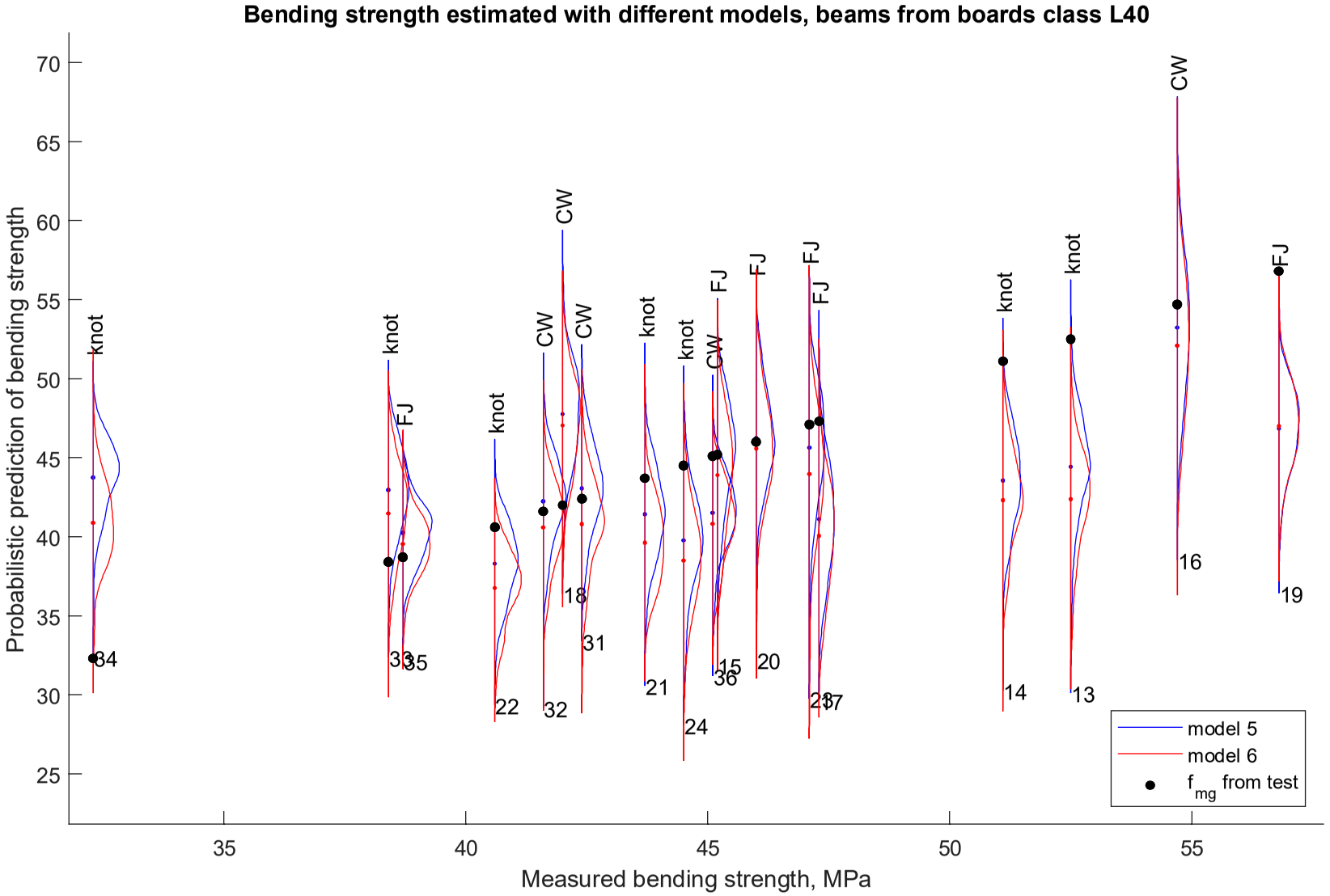

Figure A8: Bending strength distribution for beams made of lumber grade L40 from finite element model, one linear element per lamella, $\sigma_{11} = f_{t,lam}$ as failure criteria. 5 - isotropic material model, 6 - orthotropic with properties from section 4.2. FJ properties from Stadelmann (2015).

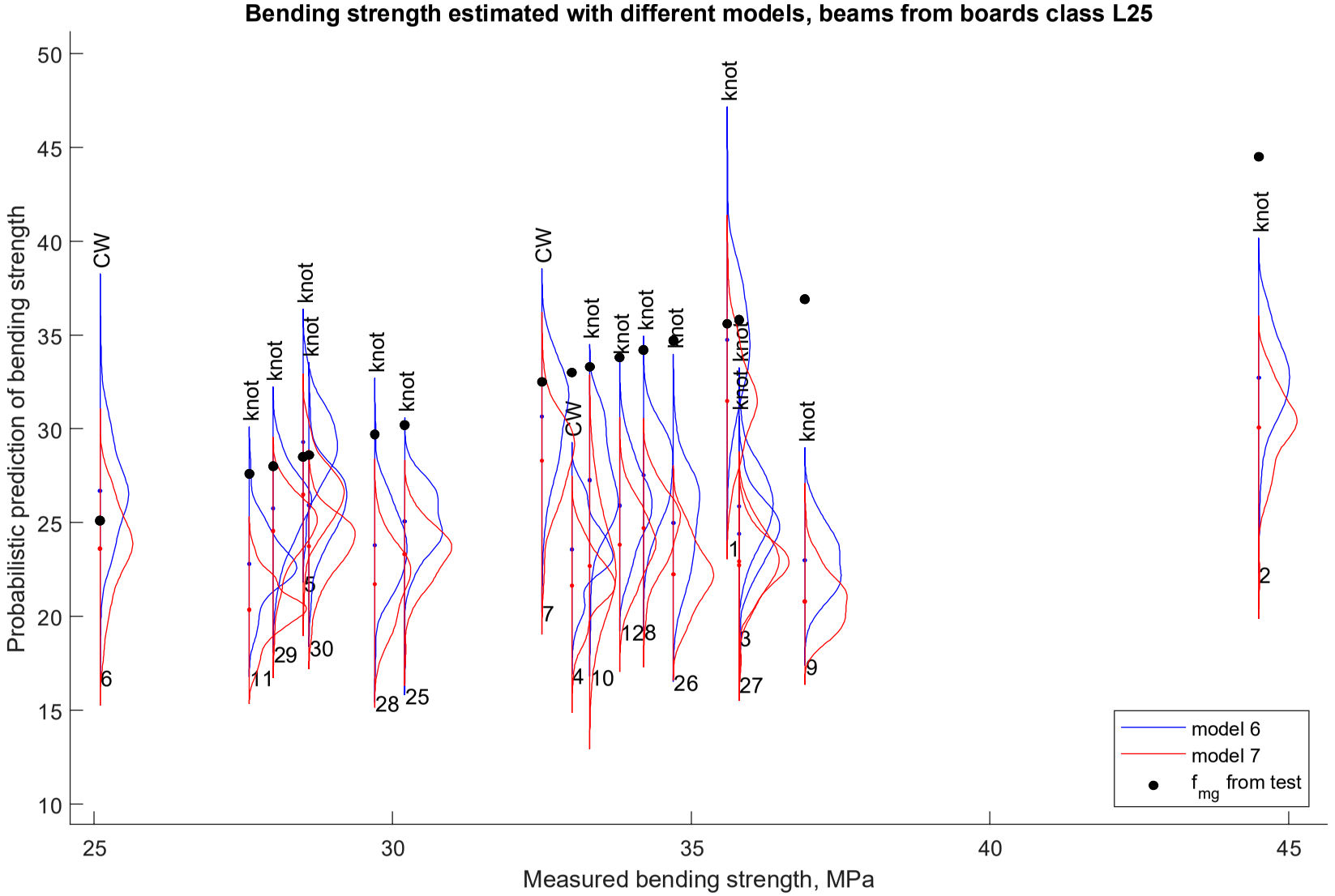

Figure A9: Bending strength distribution for beams made of lumber grade L25 from orthotropic finite element model, one element per lamella. 6 - linear elements, 7 - quadratic elements. FJ properties from Stadelmann (2015).

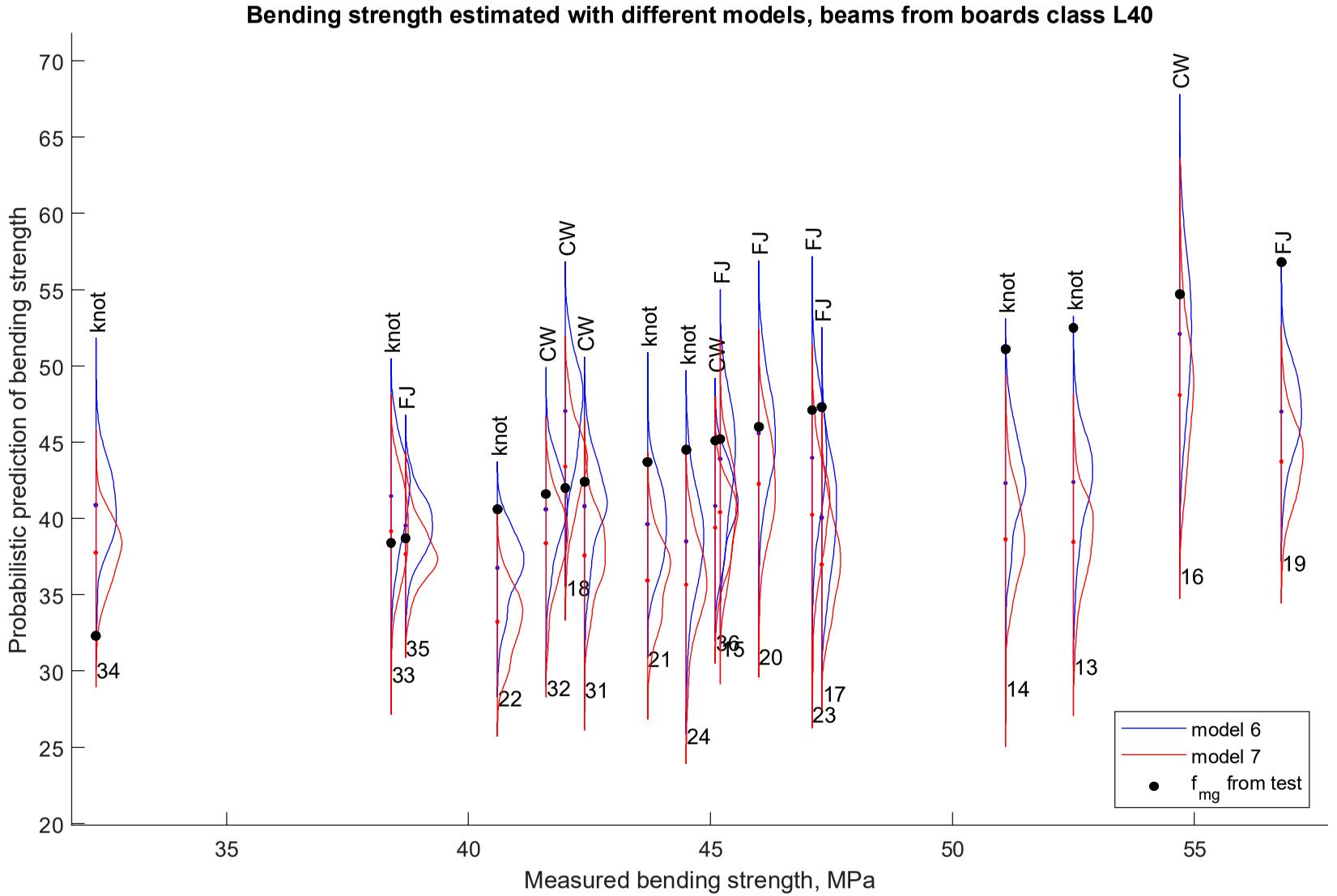

Figure A10: Bending strength distribution for beams made of lumber grade L40 from orthotropic finite element model, one element per lamella. Model 6 - linear elements, 7 - quadratic elements. FJ properties from Stadelmann (2015).

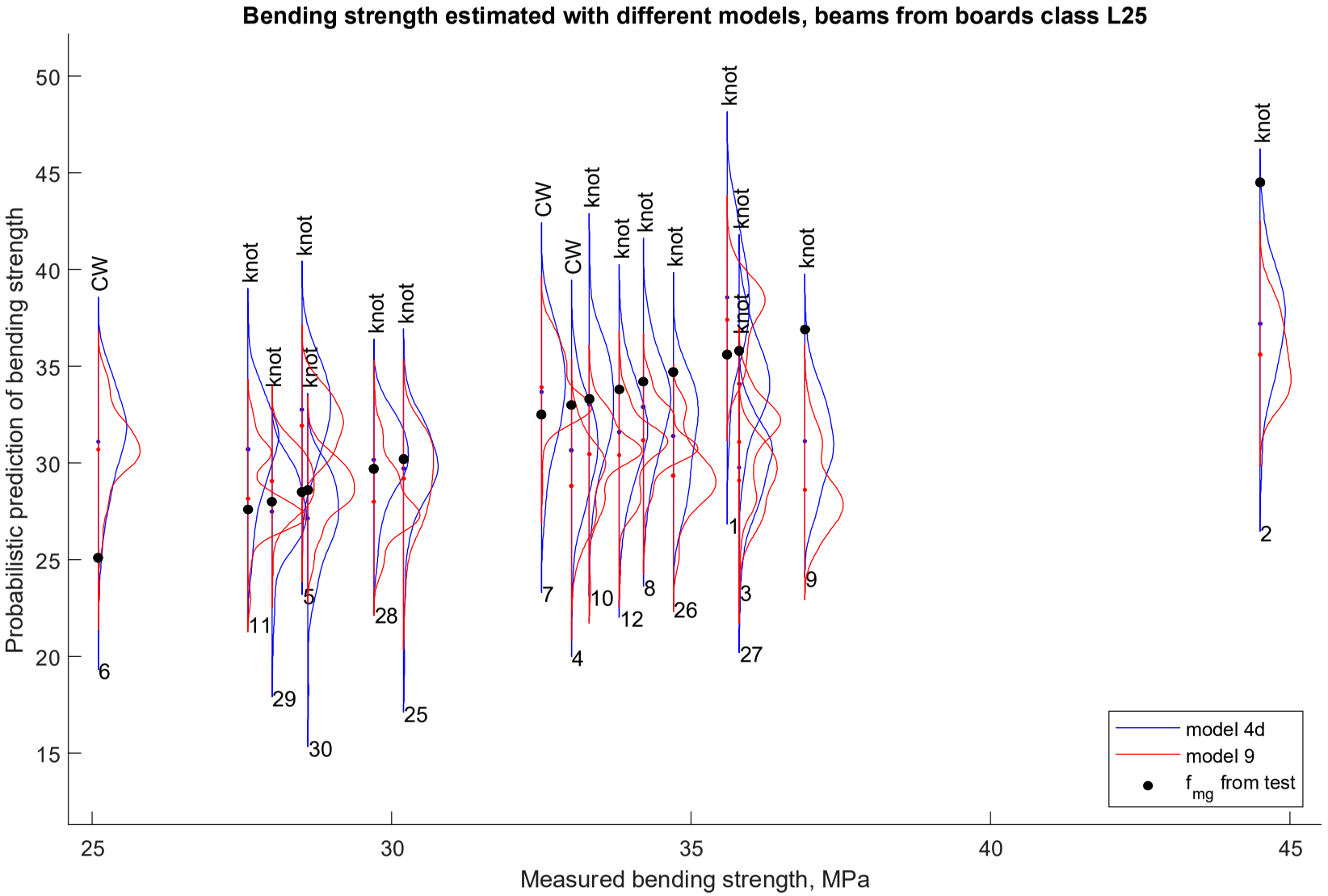

Figure A11: Bending strength distribution for beams made of lumber grade L25 from TS and FE models. Properties from Fink (2014), modified with Eq. 30. 4d - TS model, 9 - FE model, 5 elements per lamination height.

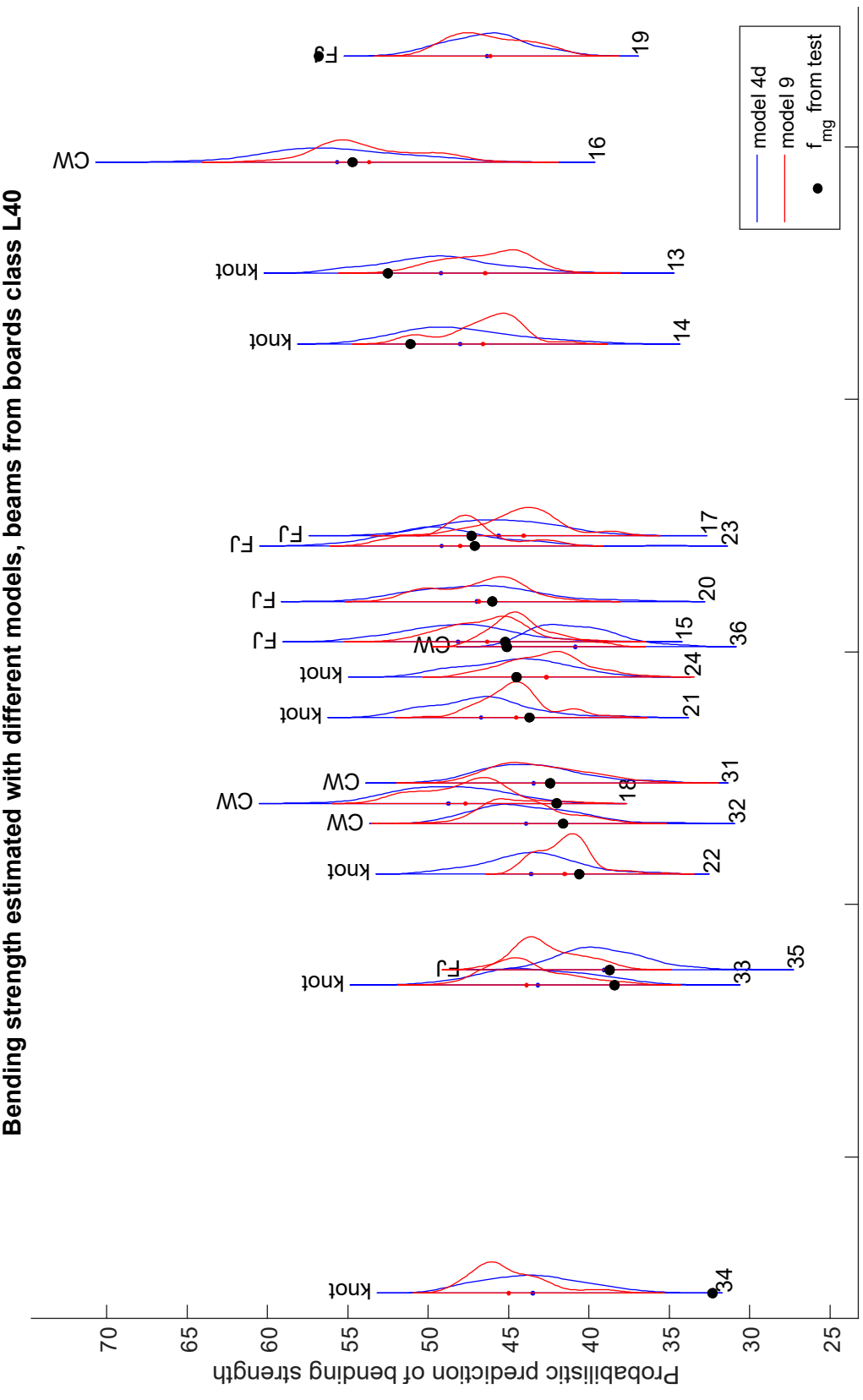

Figure A12: Bending strength distribution for beams made of lumber grade L40 from TS and FE models. Properties from Fink (2014), modified with Eq. 30. 4d - TS model, 9 - FE model, 5 elements per lamination height.

B Appendix B - Location of predicted failure

In appendix B bar graphs for type of predicted failure location is presented for selected models. Red stars show difference between bending strength from test and mean of its predictions for every beam, expressed in standard deviation of predicted strength distribution. Coefficient of variation of prediction is shown with blue dots. Beam number is shown on the top of the bars. Inside the groups (knot, FJ, CWS) bars are sorted according to mean error of model 1 and that order is kept for all models for better comparability. "Failure in upper lamellas" category in the legend refers to the setups where failure in first few iterations (or frames after failure initiation for FEM models) happend in second or upper lamellas.

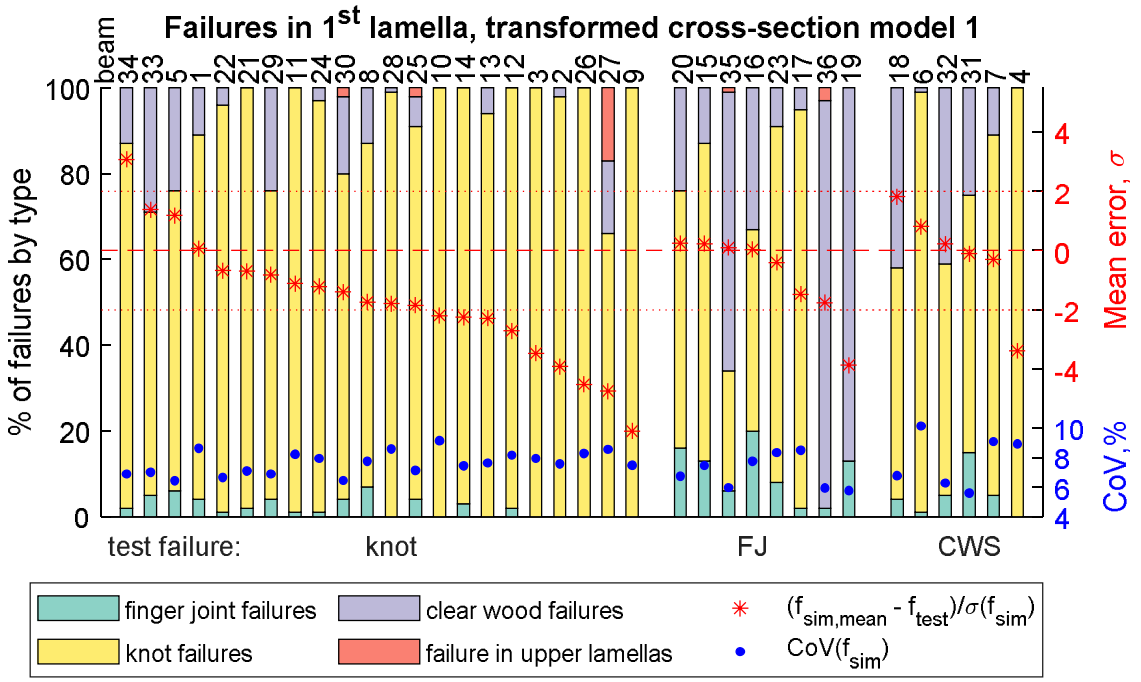

Figure B1: Location of predicted failure of the first lamella with transformed cross-section model. Wood and FJ properties from Fink (2014).

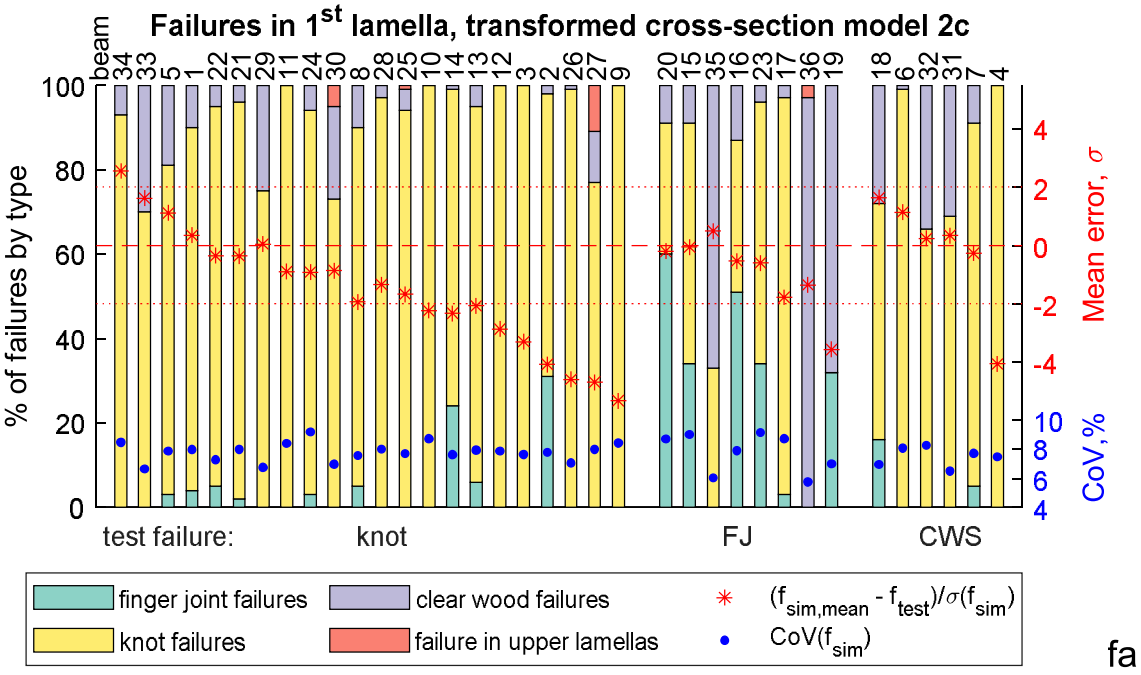

Figure B2: Location of predicted failure of the first lamella with transformed cross-section model. Wood properties from Fink (2014), model for FJ from Stadelmann (2015).

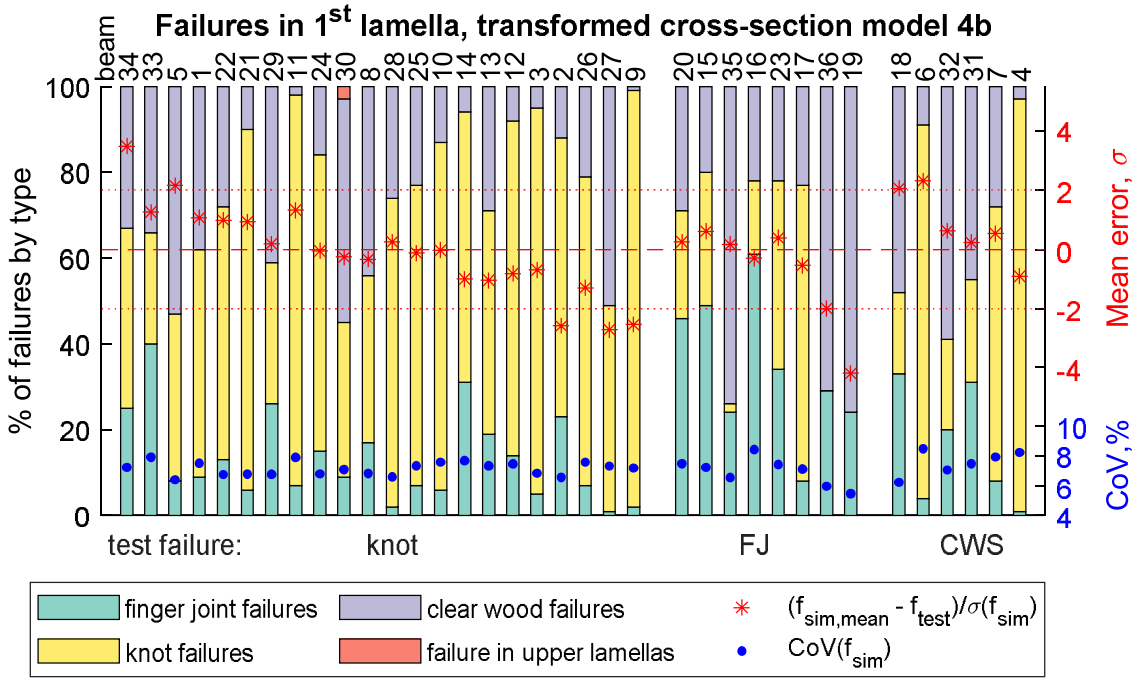

Figure B3: Location of predicted failure of the first lamella with transformed cross-section model. FJ strength properties from Stadelmann (2015). Timber strength according to Fink (2014) model, modified with Eq. 30.

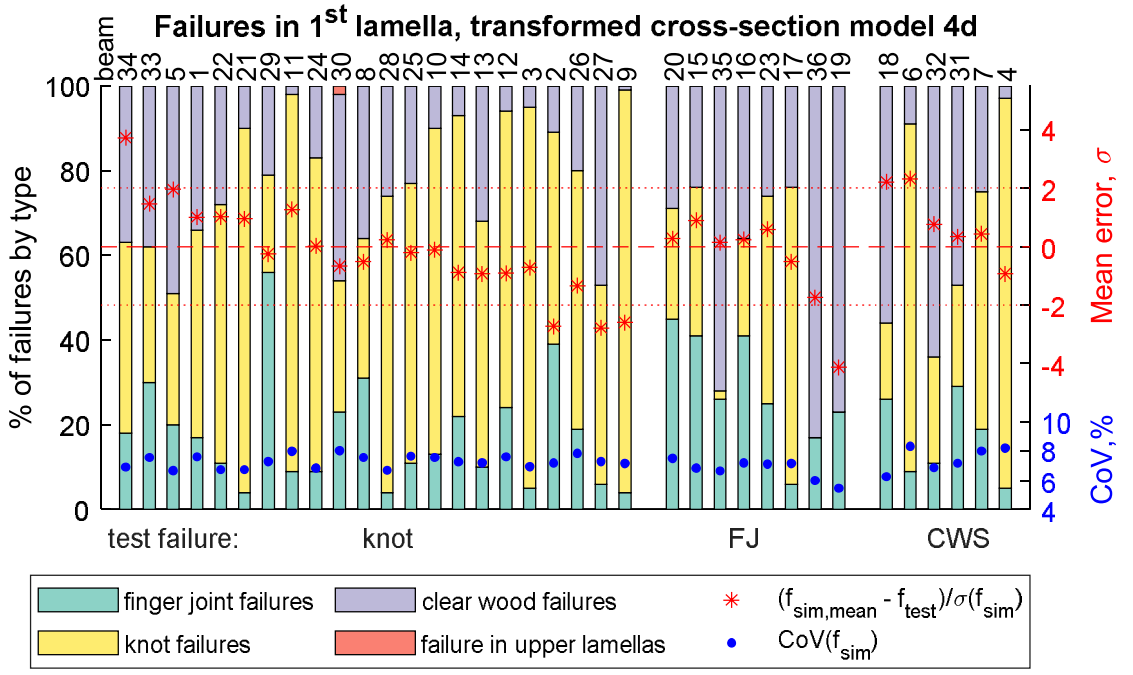

Figure B4: Location of predicted failure of the first lamella with transformed cross-section model. FJ strength properties from Fink (2014). Timber strength according to Fink (2014) model, modified with Eq. 30.

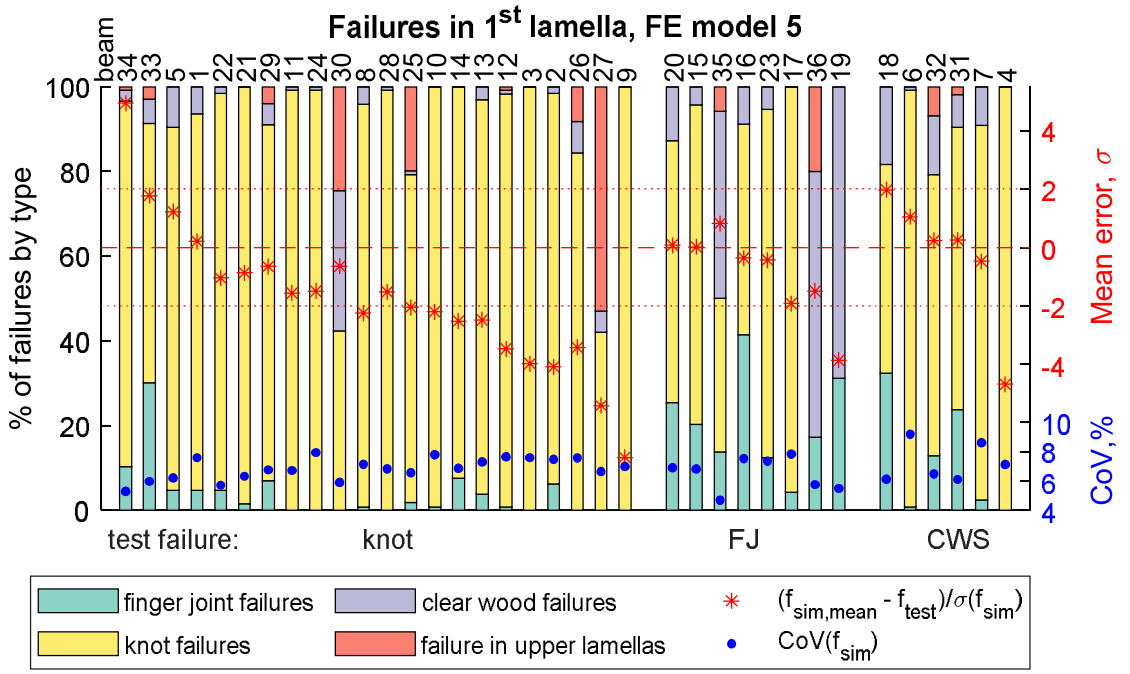

Figure B5: Location of predicted failure of the first lamella with isotropic FE model. Timber properties according to Fink (2014), FJ strength properties from Stadelmann (2015)

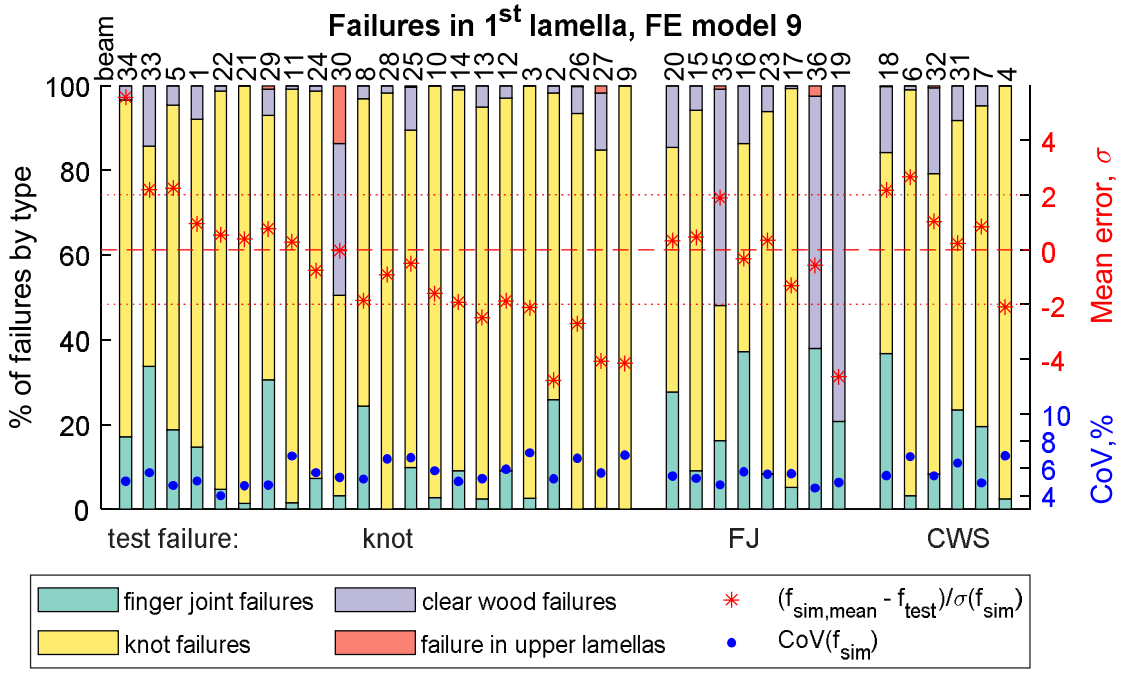

Figure B6: Location of predicted failure of the first lamella with orthotropic FEM model, linear elements, five per lamination height. Timber and FJ properties according to Fink (2014) modified with Eq. 30.